

MASTER

Nonlinear Modeling for Dynamical Analysis of 3D Directional Drilling Processes

Derksen, H.H.A.M.

Award date:
2021

[Link to publication](#)

Disclaimer

This document contains a student thesis (bachelor's or master's), as authored by a student at Eindhoven University of Technology. Student theses are made available in the TU/e repository upon obtaining the required degree. The grade received is not published on the document as presented in the repository. The required complexity or quality of research of student theses may vary by program, and the required minimum study period may vary in duration.

General rights

Copyright and moral rights for the publications made accessible in the public portal are retained by the authors and/or other copyright owners and it is a condition of accessing publications that users recognise and abide by the legal requirements associated with these rights.

- Users may download and print one copy of any publication from the public portal for the purpose of private study or research.
- You may not further distribute the material or use it for any profit-making activity or commercial gain



DEPARTMENT OF MECHANICAL ENGINEERING

Master's thesis

DYNAMICS & CONTROL - DC2021.085

Nonlinear Modeling for Dynamical Analysis of
3D Directional Drilling Processes

Name: H.H.A.M. Derksen **ID:** 1011277 **Department:** Mechanical Engineering

Thesis Supervisors:
Prof. Dr. Ir. N. van de Wouw (TU/e)
Prof. dr. E.M. Detournay (UMN)
Ir. M.F. Shakib (TU/e)

Eindhoven, September 7, 2021

Abstract

Directional drilling is a technique used to construct boreholes with complex geometries. This is needed to reach unconventional oil and gas reservoirs or to rescue uncontrollable wells. Drilling is done with the use of a long drill string to which a bottom hole assembly (BHA) is attached. This BHA contains the bit which is steered by a downhole rotary steerable system (RSS). Using this setup for drilling often results in borehole spiraling which has negative consequences for the drilling process and the borehole quality.

To show the existence and predict the onset of borehole spiraling, an analytical three-dimensional borehole propagation model (BPM) is derived. This model predicts the evolution of the borehole based on the RSS actuation. The evolution is modelled based on three components, namely (i) the bit-rock interaction (ii) a kinematic model which relates the motion of the bit to geometric variables describing the borehole and the position of the BHA, and (iii) a static model of the BHA.

The BHA consists of several stabilizers which center the drillstring in the borehole. An ideal stabilizer always contacts the borehole wall which implies that the drillstring is perfectly centered within the borehole at those stabilizers. In practice, however, the stabilizers are smaller than the borehole wall, making them so-called non-ideal stabilizers. This implies that the stabilizer either contacts the borehole wall on an arbitrary point or it floats free from the wall. This behavior has influence on the contact force. If the stabilizer floats, the contact force is zero. If there is contact, there should be a contact force. This contact force is calculated using a nonlinear complementarity approach. The BPM model which has been derived, incorporates any number of non-ideal stabilizer where each stabilizer is within a circular borehole. The BPM can be classified as a nonlinear delay complementarity system where the delay stems from the delayed influence of the borehole geometry on the deformation of the BHA.

The derived model is validated by comparison to simulations performed in literature. The simulations which are considered are responses of the borehole evolution to a step in actuation force. This is a useful analysis since such an open-loop control technique is also used in practice to steer the BHA towards its target. After a step in actuation force, the borehole evolves with a constant curvature, if the length scale is sufficiently long. These simulations also showed the onset of oscillations, which are related to borehole spiraling, after a step in actuation force. Depending on a key dimensionless parametric group, these oscillations damp out or grow unbounded since the bit-tilt is not saturated. This group includes, the active weight on the bit, properties of the BHA, bit properties including bluntness and steering resistances. Further numerical analysis showed that the inclusion of non-ideal stabilizers affects the response of the BPM significantly.

The borehole propagation model extends existing models by the inclusion of non-ideal sta-

bilizers via the framework of nonlinear complementarity problems. Moreover, it has been shown that the modeling of non-ideal stabilizers significantly affects the borehole evolution and are, therefore, crucial for the understanding of the directional drilling processes. In this model, the model is used to predict the onset of oscillations which could lead towards borehole spiraling. The prediction of the onset could serve as a basis for the design of the drilling system and also for its controls. One of the potential usages of this model is to predict the RSS force required to realize a certain borehole trajectory. Another usage could be to serve for model-based feedback controller design with the aim to accurately track borehole trajectory.

Contents

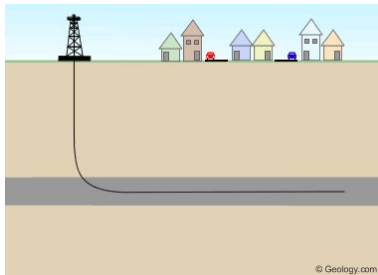
1	Introduction	1
1.1	Application of Directional Drilling	1
1.2	Directional Drilling Setup	3
1.3	Borehole Propagation Modelling	3
1.4	Literature Survey	6
1.5	Research Objectives	7
1.6	Outline	9
2	BPM	10
2.1	Modeling Asssumptions	10
2.2	Geometry	12
2.3	Loading on BHA	13
2.4	Model Components	17
2.4.1	Kinematics	18
2.4.2	Bit/rock Interface Laws	19
2.4.3	Scaling of Variables	21
2.5	BHA Model Derivation	22
2.5.1	Modelling of Non-Ideal Stabilizers	27
2.6	Borehole Propagation Model	33
3	Analysis of BPM	38
3.1	Validation	39
3.2	Effect of NIS	44
3.3	Potential	46
3.4	Discussion	48
4	conclusion	49
4.1	Conclusions	49
4.2	Recommendations	51
	Bibliography	53

1 Introduction

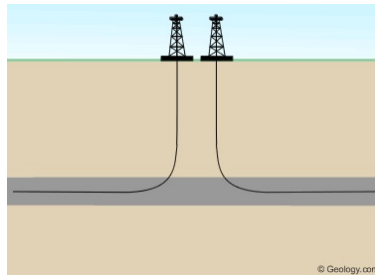
Directional drilling is a technique developed to construct boreholes that generate complex trajectories. Directional drilling happens on a large scale meaning that it drills holes reaching several kilometers in length. One can imagine that this is a time-consuming and expensive process. In this chapter, the application area of directional drilling is given. Then, the setup which is used for directional drilling is described. Next, the importance of modelling for directional drilling is discussed followed by a survey of the existing models. Finally, the research objectives of this project and the outline of this thesis are discussed.

1.1 Application of Directional Drilling

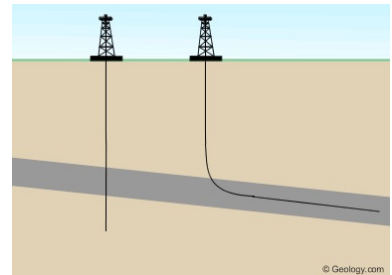
The application area in which directional drilling is used is relatively wide. Figure 1.1.1 shows six different application areas that all are related to the extraction of oil, gas, and mineral resources at hard-to-reach wells. The first application, depicted in Figure 1.1.1a, shows that directional drilling allows reaching wells which are located underneath obstacles such as cities and forests. The second application, visualized in Figure 1.1.1b, is to drill multiple wells from the same rig. This is beneficial because the rig only needs to be set up once which saves time and reduces costs. Thirdly, Figure 1.1.1c shows that directional drilling can be used to increase the pay zone of the reservoir. This is mainly used in the exploitation of shale gas because this requires a horizontal borehole due to the horizontal nature of these reservoirs. In Figure 1.1.1d, it is shown that directional drilling can be used to improve the drainage in fractured reservoirs. This is mainly done by drilling perpendicular to the fractures. Often these fractures are commonly aligned which implies that a maximum number of fractures is penetrated. Figure 1.1.1e shows that directional drilling can be used in hazardous situations to drill relief wells. One of the most famous examples of this application is the disaster that happened at the Deepwater Horizon platform in the Gulf of Mexico in 2010 [10]. After the platform called Deepwater Horizon exploded, BP drilled a relief well at 5500m below sea level using directional drilling. The objective of this relief well was to seal the troubled well that was leaking oil. In Figure 1.1.1f, it is shown that directional drilling can be used to install underground facilities when excavation is not an option. The installation of water, gas, and electricity supply needs the installation of pipes. To this end, directional drilling is an enabling technique. Another application of directional drilling is avoiding geological fractures in the earth mass since this could create damage on the well due to the earth's tectonic movement [27]. Besides these, directional drilling can also be used to drill around



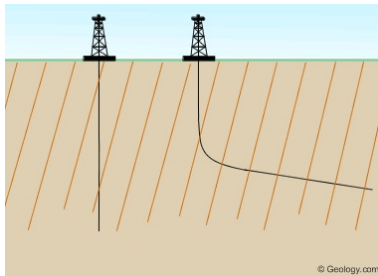
(a) Drilling of a borehole underneath obstacles such as cities or forests.



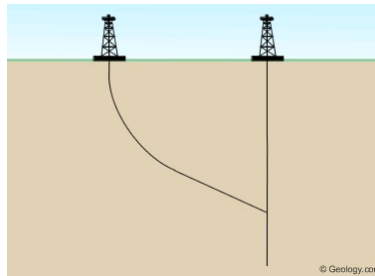
(b) Drilling multiple boreholes from the same rig.



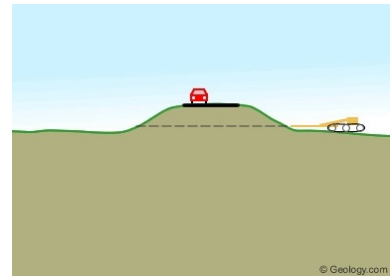
(c) Increase the pay zone of a reservoir by drilling horizontally.



(d) Drilling to improve the drainage in a fractured well.



(e) Drilling to rescue uncontrollable wells.



(f) Installment of underground facilities.

Figure 1.1.1: Various applications of directional drilling. Figures reprinted from [12].

hard rock formations in order to prevent the drill bit from wearing fast, which saves money and time due to the expensive process of replacing the drill bit. Lastly, directional drilling is used in the geothermal and mining industries [23].

1.2 Directional Drilling Setup

The directional drilling setup consists of several components, as described next. Figure 1.2.1a shows the setup, which consists of a rig, drillstring and bottom hole assembly (BHA). The drillstring is a hollow slender tube typically of order of 1-10km in length. This string is suspended at the rig which is located at the earth's surface area. The rig imposes the rotary speed and axial force (hook-load) on the drillstring. Due to its own weight, most of the drillstring is in tension. Only the bottom part of the drillstring is under compression due to the weight of the drillstring and its own weight and it is called the bottom hole assembly (BHA). The BHA is typically a couple hundred metres long. It is important that this part is under compression in order to apply a high enough pressure onto the drill bit. There are several components in the BHA which play an important role in the borehole evolution. Firstly, the stabilizer's function is to centre the BHA in the middle of the borehole. Usually a BHA is equipped with three to five stabilizers. A stabilizer is a short element with a larger diameter, as depicted in Figure 1.2.1d. The second important element is the Rotary Steering System (RSS), which is a semi-automated tool that is able to steer the BHA while rotating. There are two main types of RSS. The first is a push-the-bit system which only applies a lateral force, pushing against the borehole via extensible pads. The other system is a point-the-bit system where the bit is tilted into a certain orientation such that the desired trajectory is achieved. In Figure 1.2.1b, a push-the-bit RSS system is depicted. In Figure 1.2.1c, the push-the-bit RSS is depicted, axially. This tool is placed between the bit and the first stabilizer. At the end of the BHA, a polycrystalline diamond compact (PDC) drill bit, visualized in Figure 1.2.1e, is located to drill into the rock formation. This type of bit is favorable for directional drilling for its ability to drill large curvature boreholes.

1.3 Borehole Propagation Modelling for Directional Drilling

Directional drilling is a time-consuming and expensive process. To optimize the drilling procedure in terms of reducing time and costs and enhancing accuracy the drill bit should go to the desired location in a fast and accurate manner. A borehole propagation model contributes positively to optimize the drilling process. A borehole propagation model predicts the evolution of the borehole into the earth based on known forces and actuation forces. Using such a model, the root cause of observed behavior in practice can be analyzed. Potentially, if the root cause is understood, the BHA design or control can be improved such that undesired phenomena do not occur anymore or their occurrence is reduced.

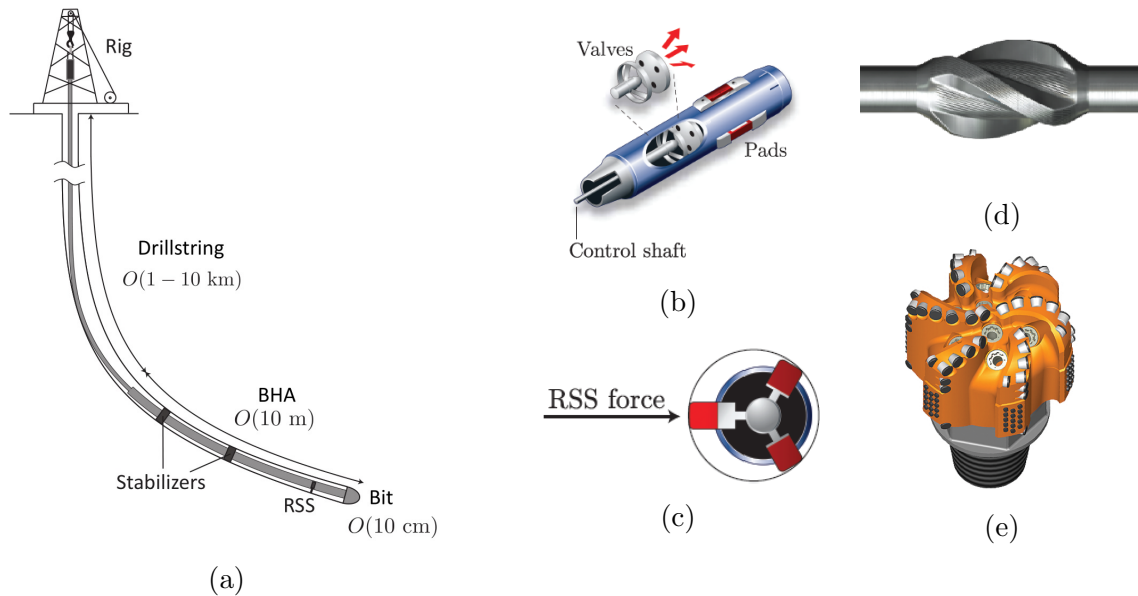


Figure 1.2.1: Overview of a directional drilling system. Subfigure (a) shows the complete drilling system, subfigure (b) shows the push-the-bit Rotary Steering System (RSS) used for steering, subfigure (c) shows an axial view of the RSS, subfigure (d) shows a stabilizer equipped on the BHA and subfigure (e) shows the polycrystalline diamond compact (PDC) bit used for cutting into rock formations. Figures reprinted from [23] and [15].

An interesting undesired behavior observed in measured field data is self-excited, instability-induced borehole oscillations, called borehole spiraling, visualized in Figure 1.3.1. This figure shows that the borehole has a corkscrew-like shape in three dimensions (3D). The 2D projection of this 3D phenomenon is called borehole rippling, which consists of oscillations in the xz -plane as visualized in Figure 1.3.1a. The borehole spiraling phenomenon measured from field data, is shown in Figure 1.3.1b.

Borehole spiraling is undesired because it has a lot of negative consequences. The first consequence is that the corkscrew-shaped borehole makes it more difficult to insert a casing. This casing is important to make sure the borehole does not collapse. A second consequence is increased drag forces which leads to a low rate-of-penetration which makes the process more time consuming. This low rate-of-penetration does accelerate the bit wear which decreases efficiency and thus results in larger costs. Also changing the bit because it has worn too much is a time consuming and costly process. Thirdly, the accuracy of reaching the desired target position is reduced.

A second phenomenon different from spiraling is that the trajectory is sometimes counterintuitive where the borehole tends to steer opposite to what is intended by the RSS [23]. This could be a negative phenomenon, but can also be exploited if understood. As aforementioned, the root cause of these phenomena could be analyzed in a model. If this root cause is known, the BHA design or BHA control could be improved such that these phenomena disappear or decrease in intensity.

Another use of a borehole propagation model is to design feedback controllers that track a certain borehole trajectory as done by [7, 19, 27, 30]. One way to regulate the borehole orientation in an open-loop manner by an operator [19], is via command messages to the RSS based on the downhole measurements. These messages contain a desired inclination and azimuth angle. Then, the command messages are converted into a constant RSS force which is subsequently applied. A constant RSS actuation leads to a borehole with constant curvature if the length scale is sufficiently long. This way of controlling has the consequence that deviations from the target location can occur which have to be corrected by the operator. This also implies that the experience of drill-operators is highly important. A model could be used to develop a model-based controllers, for example, robust controllers [27] or model predictive control [30]. If the borehole evolution can be controlled in this way, the costs could be reduced because the system becomes more autonomous [7]. The performance of model-based controllers depends on the accuracy of the borehole propagation model. Therefore, it is important to develop models that capture, or at least predict, the occurrence of the aforementioned phenomena.

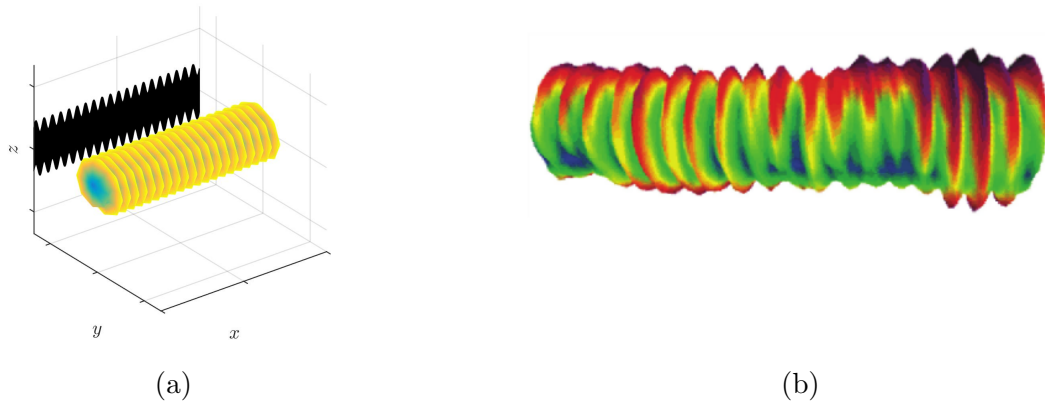


Figure 1.3.1: Illustration of borehole spiraling. In (a) borehole spiraling is shown in three dimensions (x, y, z) , and also the two-dimensional $(xz$ -plane) equivalent called rippling is depicted. In (b), a reconstruction of borehole spiraling from measured data is shown. Figure (a) reprinted from [15] and (b) from [26].

1.4 Literature Survey

The literature survey gives an overview of the different type of models which already exist. There are two main types of borehole propagation models derived in the past, namely numerical and analytical. The numerical models make use of finite-element methods to predict the trajectory of the borehole [2, 4–6, 9, 17, 18, 21, 24]. These models do not provide essential insights into relevant parameters of directional drilling and, therefore, give limited insight into the physics of borehole propagation, caused by the parameters not having a physical meaning. Consequently, such models lack transparency in terms of the effect of model parameters and RSS actuation on the borehole propagation.

The models which do give more insight into the essential underlying physics of the borehole propagation are the analytical models. The first step towards these analytic models is made by Lubinski and Woods [14]. They derived an analytical model for the interaction between the bit and the rock and the interaction between the BHA and its surroundings. Later on, Neubert and Heisig [20] derived the equations governing the borehole evolution in directional drilling for cases where a point-the-bit RSS actuation is used. For the BHA model, they used an Euler-Bernoulli beam model instead of a finite-element model that were used in the numerical models. This model was altered by Downton and Ignova [8]. They derived a model that is restricted to small rotations with respect to the borehole evolution.

Analytical models that derive the equations governing the evolution of the directional drilling

have been derived later on. An overview of these models is given in Figure 1.4.1. The first model, derived by [22], describes the borehole evolution in two dimensions. This model is indicated with A in the figure. In this propagation model, the evolution of the borehole is described by a set of delay differential equations where the states are chosen to be the inclination and the azimuth of the borehole. An extension to this model is done by [23] to the three-dimensional case, indicated by B . The models A and B can predict instability-induced oscillatory behavior, that can be related to the onset of the borehole rippling and spiraling. These oscillations, however, grow unbounded in models A and B because the bit tilt can not saturate. These models, however, do not incorporate bit tilt saturation which is shown to be observed in practice according to [15]. Bit tilt is the orientation difference between the bit and the borehole at the bit as visualized in Figure 1.4.2. Therefore, the inclusion of bit tilt saturation in borehole propagation models is done in both two and three dimensions by respectively [22] and [15] leading to models A^* and B^* . Due to the inclusion of the bit tilt saturation in models A^* and B^* , these models are able to predict steady-state oscillations that are related to borehole rippling and spiraling. This prediction is made based on a linear stability analysis performed in [16].

The models A^* and B^* consider the case with idealized stabilizers, which always make contact with the borehole walls. In practice, however, the stabilizers are smaller than the borehole wall. This is due to undergauged stabilizer by design, hole enlargement by erosion of the mud and whirling of the BHA. Therefore, non-ideal stabilizers need to be incorporated in the model. A non-ideal stabilizer is a stabilizer that either touches the borehole wall or not at all as visualized in Figure 1.4.2. A model that includes non-ideal stabilizers instead of ideal ones is derived by [26], indicated with C in the figure. In that work, a two-dimensional model with the inclusion of bit tilt saturation and an arbitrary number of non-ideal stabilizers model is derived. In addition to capturing the steady-state oscillations related to borehole rippling, model C shows significantly different behavior, including the counter-intuitive behavior discussed earlier, when the non-ideal stabilizer either touches or stays clear from the borehole. Furthermore, due to the inclusion of non-ideal stabilizers, this model also shows that under application of a constant RSS force, there exist different attractive steady-state solutions. In [26], the model for the BHA is presented completely analytically in the form of a so-called linear complementarity system [3]. Independently, non-ideal stabilizers are also modeled in the three-dimensional case by [29]. In that work, the authors also use the linear complementarity problem framework to model non-ideal stabilizers. Their method, however, approximates the intersection of the drilled borehole to be square, rather than a circle or ellipsoid which would be closer to reality.

1.5 Research Objectives

As aforementioned, modeling directional drilling serves multiple purposes such as understanding behavior which is observed in practice and the design of model-based feedback controllers.

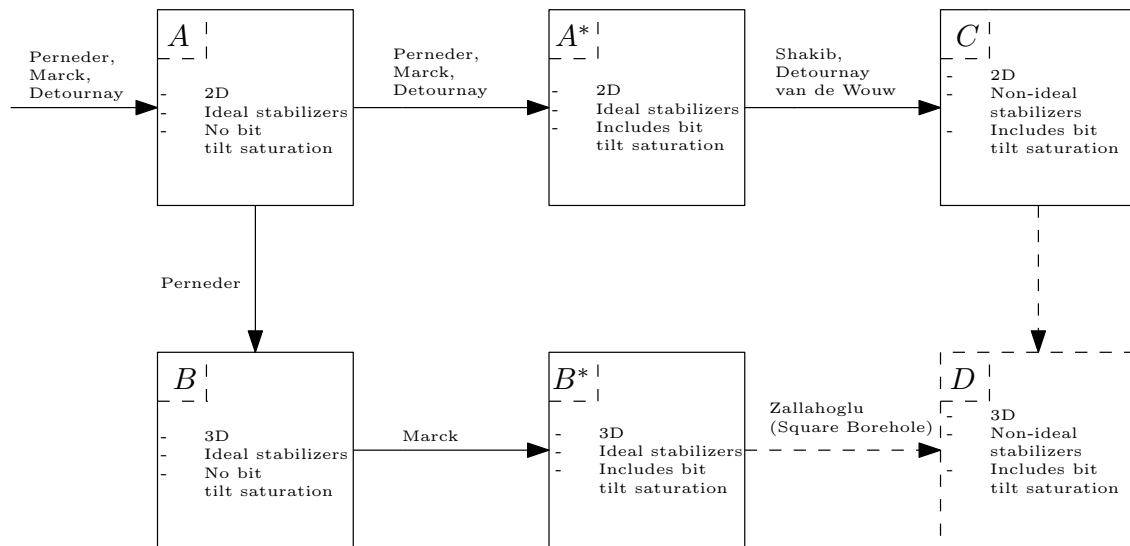


Figure 1.4.1: An overview of analytic borehole propagation models.

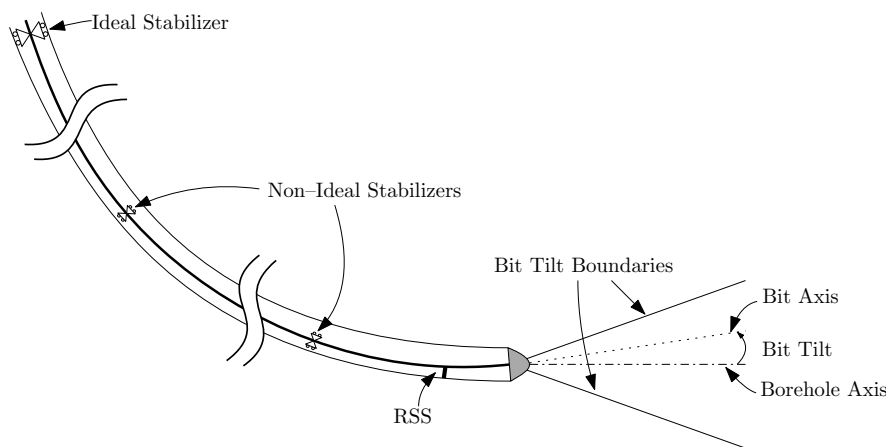


Figure 1.4.2: Overview of the geometry of the BHA showing the non-ideal stabilizers, the definition of bit tilt, and the bit tilt saturation.

The current model labeled with C in Figure 1.4.1 describes the borehole propagation of directional drilling with the inclusion of non-ideal stabilizers and bit tilt saturation in a 2D plane. As aforementioned, model C is modeled with the use of linear complementarity problem which has an advantage that it provides, for any number of stabilizers, a closed-form expression for the dynamics governing the borehole evolution.

In reality, however, the drilling process happens in three dimensions. Therefore, it is required to extend the model C from the planar case to the three-dimensional case into model D . This extension is partly done by [29]. That model, however, considers the stabilizers to be in a square borehole, which is not realistic, instead of a circular or ellipsoidal borehole. It is important that the non-ideal stabilizers are modelled in the circular borehole. The insight gained from such a model can then be used to improve the design of the BHA and for controller design.

The objectives of this thesis are as follows:

- Model the borehole evolution in three dimensions, including any number of non-ideal stabilizers, where the stabilizers are located in a circular/ellipsoidal borehole. This is model D in Figure 1.4.1.
- Perform a numerical study to validate the derived borehole propagation model with existing models in literature.
- Perform a numerical study to predict the onset of oscillations in a 3D scenario, related to borehole spiraling.

The inclusion of the bit tilt saturation is out of the scope of this thesis and is left for future work.

1.6 Outline

The equations governing the borehole evolution are described in Chapter 2. This is based on a BHA containing an arbitrary number of non-ideal stabilizers, to obtain model D . Then, in Chapter 3, a numerical validation of the model is done by comparison to the two-dimensional model from [26]. Furthermore, this chapter also discusses the influence of the non-ideal stabilizers on the borehole evolution. Lastly, this chapter also discusses what the potential usage of the model is. In Chapter 4 the conclusions of the research is given and also recommendations for future work.

2 Borehole Propagation Model

This chapter presents the derivation of the borehole propagation model. Firstly, the modeling assumptions are mentioned in Section 2.1. This is followed by Section 2.2, which describes the geometry of the borehole and the BHA. Subsequently, Section 2.3 describes the forces and moments which act on the BHA. Then, Section 2.4 elaborates on the different model components and the relation between those components. This section also gives a detailed explanation of each component. Fifthly, Section 2.5, describes the derivation of the BHA model. Lastly, Section 2.6 describes the borehole propagation model model.

2.1 Modeling Assumptions

To model the borehole propagation, assumptions and hypotheses are needed. An overview, mainly taken from [23], of these assumptions is given in this section. These assumptions are commonly used in borehole propagation models [15, 26].

The first hypothesis adopted is that the propagation of the drilling process can be averaged over several revolutions. This is justified by the time scale at which the propagation process takes place. The bit penetration per revolution is of order $\mathcal{O}(1 \text{ mm/revolution})$. The model resolution is of order $\mathcal{O}(10^{-1} \text{ m})$ which corresponds with the dimension of the bit. Due to this large difference in order magnitude, it is justified that the process is averaged over several revolutions. This also implies that the axial angular position of the bit is not important. Another consequence of this hypothesis is that dynamical processes at a time scale smaller than a revolution of the bit can be disregarded. They either do not influence the drilling direction or they can be lumped into parameters of the model. Stick-slip oscillations of the bit and whirling of the bit are examples of such dynamical processes that are neglected [26].

The second hypothesis adopted is that the propagation direction is rate independent for a range of bit angular velocity of order $\mathcal{O}(10 \sim 100 \text{ revolutions/min})$. This is justified by the rate-independent nature of the bit/rock interface laws [22]. In these laws, the dominant variable is the amount of rock removed per revolution. An important consequence of this hypothesis is that time is not a suitable variable to track the evolution of the borehole. Instead, the borehole length is used to track the evolution hole shape.

Lastly, to model borehole propagation in directional drilling, it is sufficient to consider only the BHA. The effect of the drillstring is lumped into contact forces at the upper boundary of the BHA, corresponding to the position of the last stabilizer. In practice, it is seen that the lateral forces and moments at the bit influence the drilling direction predominantly. These forces and moments at the bit are mainly affected by the first three or four stabilizers.

Alongside these hypotheses, a set of assumptions is adopted to idealize the model:

- The bit-rock interface laws pertain to homogeneous and isotropic rock formations. This means that the properties of the rock formation do not change over the borehole length and the drilling direction.
- The BHA has a uniform distributed weight and uniform flexural rigidity. The BHA is modeled from the bit to the last stabilizer.
- All stabilizers are (potentially) non-ideal, except for the last one, which means that each stabilizer either touches the borehole wall or not at all. These contacts are modeled as contact points and thus do not transmit any moment between the BHA and the borehole wall.
- The internal moment at the last stabilizer is assumed to be zero.
- The stabilizers, RSS, and the bit are the only contact points between the borehole wall and the BHA. It is assumed that there is no additional contact between the BHA and the borehole wall. This assumption is valid as long as the deformation of the BHA is sufficiently small to avoid additional contact points.
- The RSS is a push-the-bit system which implies that it applies a lateral force on the BHA. This assumption is valid as long as the pads of the RSS are not fully extended. If all the pads would be fully extended, the RSS would form a displacement constraint. The RSS is located between the bit and the first stabilizer.

A second set of assumptions is adopted to simplify and linearize the mathematical formulation:

- The radius of curvature of the borehole is large compared to the length of the BHA. Only the first 20 \sim 30 (\sim 100ft) meters significantly influence the drilling tendency. In industry, the borehole curvature is measured by a so-called built-rate, which is the increase of inclination over a length of ± 30 meter of the borehole. For a push-the-bit RSS, the maximum built rate is $6^\circ/100\text{ft} \approx (6^\circ/30\text{m})$ which corresponds to a curvature radius of 280 m. Therefore, the contact forces can be assumed to be orthogonal to the undeformed reference configuration of the BHA, which simplifies the BHA modeling. Furthermore, the direction of gravity (relative to the BHA axis) can be taken constant over the entire BHA.
- The BHA axis is a small perturbation of the borehole axis at the length scale of the BHA. This assumption is justified by the small clearance of order $\mathcal{O}(1\text{ cm})$ between

the BHA and the borehole walls compared to the length of the BHA. This observation combined with the previous assumptions implies that the geometrical nonlinearity in the BHA is negligibly small. As a consequence, the Euler-Bernoulli theory for the bending of a beam is adopted to model the deformation of the BHA inside the borehole.

- The axial force and torque on the BHA are at least an order of magnitude smaller than the loads that would induce buckling of the BHA. The typical axial strains of the BHA are of order $\mathcal{O}(10^{-4})$ which allows assuming that the BHA is not extensible.

2.2 Geometry

An overview of the geometry description is given in Figure 2.2.1. At the rig, an earth-fixed frame \vec{e} is defined such that \vec{e}_z points in the direction of gravity. The vectors \vec{e}_x and \vec{e}_y span a square on the surface area. The borehole is a cylindrical object defined by its central axis \mathcal{B} and its varying cross section. The central axis \mathcal{B} is parameterized by the curvilinear coordinate S . For S , it holds that $S = 0$ is located at the rig and $0 \leq S \leq L$, where L is the increasing length of the borehole and also the evolution variable of the BPM. The central axis \mathcal{B} is formally defined as the trajectory of the reference point at the bit, which is incorporated in the vectorial function $\vec{R}(S)$. This function is continuous in S but only piecewise continuously differentiable as sudden changes in orientation can occur. The tangent to the borehole

$$\vec{I}_1 = \frac{d\vec{R}}{dS} \quad (2.2.1)$$

uniquely defines the inclination $\Theta(S) \in [0, \pi]$ and the azimuth $\Phi(S) \in [0, 2\pi)$. The inclination is measured with respect to \vec{e}_z and the azimuth with respect to \vec{e}_x in a clockwise direction as can be seen in Figure 2.2.1. The local reference frame \vec{I} , attached to the borehole, is defined according to a rotation matrix $\underline{A}_I(\Phi, \Theta)$ which relates $\vec{I} = \underline{A}_I \vec{e}$. This matrix is given as

$$\begin{aligned} \underline{A}_I(\Phi, \Theta) &= \begin{bmatrix} c_\Theta & s_\Theta & 0 \\ -s_\Theta & c_\Theta & 0 \\ 0 & 0 & 1 \end{bmatrix} \begin{bmatrix} 1 & 0 & 0 \\ 0 & c_\Phi & s_\Phi \\ 0 & -s_\Phi & c_\Phi \end{bmatrix} \begin{bmatrix} 1 & 0 & 0 \\ 0 & c_{-\frac{1}{2}\pi} & s_{-\frac{1}{2}\pi} \\ 0 & -s_{-\frac{1}{2}\pi} & c_{-\frac{1}{2}\pi} \end{bmatrix} \begin{bmatrix} c_{-\frac{1}{2}\pi} & 0 & -s_{-\frac{1}{2}\pi} \\ 0 & 1 & 0 \\ s_{-\frac{1}{2}\pi} & 0 & c_{-\frac{1}{2}\pi} \end{bmatrix} \\ &= \begin{bmatrix} c_\Phi s_\Theta & s_\Phi s_\Theta & c_\Theta \\ c_\Phi c_\Theta & s_\Phi c_\Theta & -s_\Theta \\ -s_\Phi & c_\Phi & 0 \end{bmatrix}, \end{aligned} \quad (2.2.2)$$

where respectively s and c represent the sin and cos function with the argument as in the subscript. Initially, the frame \vec{I} needs a permutation with respect to \vec{e} , such that \vec{I}_1 is coaxial with \vec{e}_z , \vec{I}_2 with \vec{e}_x , and \vec{I}_3 with \vec{e}_y . This permutation accounts for the two constant matrices in (2.2.2). Then, two elementary rotations are performed that are characterized by the rotation matrix \underline{A}_I . The first elementary rotation is a rotation of azimuth Φ around \vec{e}_1 ,

followed by a second elementary rotation of inclination Θ around \vec{e}_3 . With this definition for \vec{I} , \vec{I}_1 is tangent to the borehole, \vec{I}_2 is in the same vertical plane as \vec{I}_1 and for \vec{I}_3 holds that $\vec{I}_3 = \vec{I}_1 \times \vec{I}_2$.

The BHA axis, \mathcal{D} , is a small perturbation of the borehole axis \mathcal{B} . For a certain borehole length L , \mathcal{D} is parameterized by the curvilinear coordinate s with the origin at the bit. It is described by the vectorial function $\vec{r}(s, L)$. The function \vec{r} is continuously differentiable with respect to s , but only piecewise continuously differentiable with respect to L . At the bit, where $s = 0$, a local reference frame \vec{i} is attached. The unit vector \vec{i}_1 is tangent to the BHA axis \mathcal{D} and in itself a small perturbation of \vec{I}_1 . This tangent vector \vec{i}_1 has an inclination of $\theta(s, L) \in [0, \pi]$ and azimuth $\phi(s, L) \in [0, 2\pi)$. Furthermore, the frame \vec{i} is also defined by a rotation matrix $\underline{A}_i(\phi, \theta)$, characterizing a rotation of \vec{i} with respect to the earth-fixed frame \vec{e} at the position of the rig. This rotation matrix is the same as (2.2.2), however, evaluated at θ and ϕ rather than Θ and Φ , respectively. For \vec{i} , it also holds that \vec{i}_1 is the bit axis tangent to the BHA axis, \vec{i}_2 is in the same vertical plane as \vec{i}_1 and \vec{i}_3 is given by $\vec{i}_3 = \vec{i}_1 \times \vec{i}_2$.

Finally, a third reference frame is defined \vec{I} with respect to the BHA. The forces and moments acting on the bit are expressed in this frame. In this frame, \vec{I}_1 is aligned with chord C_1 , which is the link between the center of the borehole at the bit $\vec{r}(0, L)$ and at first stabilizer $\vec{r}(s_1, L)$. Vector \vec{I}_2 is in the same vertical plane as \vec{I}_1 and $\vec{I}_3 = \vec{I}_1 \times \vec{I}_2$. The inclination and azimuth of chord C_1 are respectively $\langle \Theta_1 \rangle$ and $\langle \Phi_1 \rangle$.

In total, three frames are introduced, namely \vec{I} , \vec{i} and \vec{I} . Reference frame \vec{I} is introduced to track the borehole geometry. This frame is defined by the inclination and azimuth angles Θ and Φ . On the one hand, angle Θ measures the angle between \vec{e}_z and \vec{I}_1 , on the other hand, angle Φ measures the angle between \vec{e}_x and the projection of \vec{I}_1 in the (\vec{e}_x, \vec{e}_y) plane. Bit frame \vec{i} is used to express the forces and moments acting on the bit. Besides that, it also defines the orientation of the bit within the borehole. This frame is defined by the inclination and azimuth angles θ and ϕ , respectively. On the one hand, angle θ measures the angle between \vec{e}_z and \vec{i}_1 , on the other hand, angle ϕ measures the angle between \vec{e}_x and the projection of \vec{i}_1 in the (\vec{e}_x, \vec{e}_y) plane. The BHA frame \vec{I} is used to express the forces and moments acting on the BHA. This frame is defined by the inclination and azimuth angles $\langle \Theta \rangle$ and $\langle \Phi \rangle$, respectively. On the one hand, angle $\langle \Theta \rangle$ measures the angle between \vec{e}_z and chord $C_{(1)}$, on the other hand, angle $\langle \Phi \rangle$ measures the angle between \vec{e}_x and chord $C_{(1)}$ in the (\vec{e}_x, \vec{e}_y) plane.

2.3 Loading on BHA

The BHA is considered as a slender elastic object subject to external forces and moments. The stabilizers are numbered from 1 until n starting with the stabilizer closest to the bit. A schematic overview of a n -stabilizer BHA in both the (\vec{I}_1, \vec{I}_2) and (\vec{I}_1, \vec{I}_3) plane, including

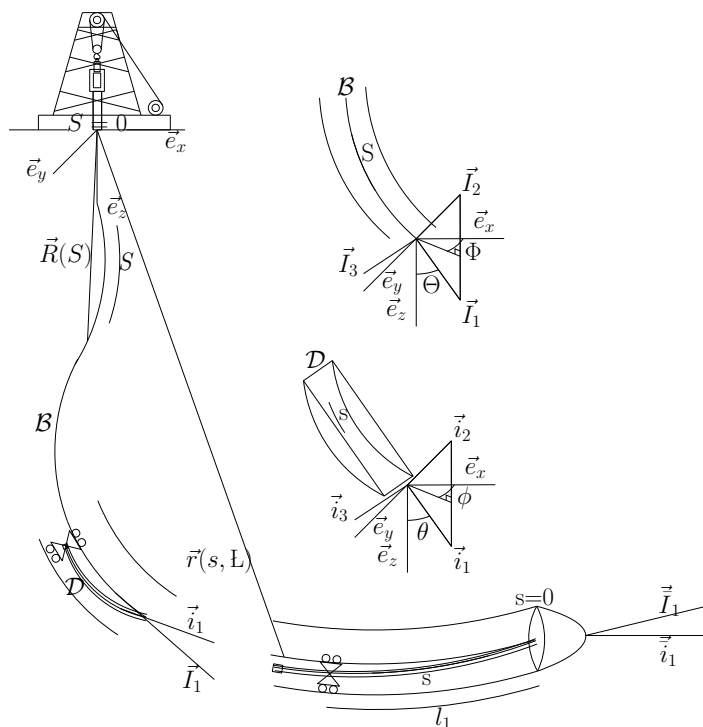


Figure 2.2.1: The geometry description of the BHA.

these forces and moments is given in Figure 2.3.1. The distance between the bit and the first stabilizer is defined as $\ell_{(1)}$. Subsequently, the distance between the $(i-1)$ -th and the i -th stabilizer is defined as $\ell_{(i)}$ for $i = 2, \dots, n$. Since the BHA is inextensible, the curvilinear coordinate s remains the arc length and thus the position of the i -th stabilizer is always given by

$$s_i = \sum_{k=1}^i \ell_{(k)} \quad \text{for } i = 1, 2, \dots, n. \quad (2.3.1)$$

A chord $C_{(1)}$ is defined as the straight line segment between the bit and the center of the borehole at the first stabilizer. Subsequently, chords $C_{(i)}$, for $i = 2, 3, \dots, n$, define the straight line segment between the borehole centers at s_{i-1} and s_i . Each chord has its own inclination $\langle \Theta \rangle_{(i)}$ and azimuth $\langle \Phi \rangle_{(i)}$, which is the average inclination and azimuth, respectively, of the borehole over the BHA segment between s_{i-1} and s_i . The inclination and azimuth alter over the evolution variable, which is the borehole length denoted with \mathbf{L} . The average inclinations and azimuths can be calculated by

$$\langle \Theta \rangle_{(i)}(\mathbf{L}) := \frac{1}{\ell_{(i)}} \int_{s_{i-1}}^{s_i} \Theta_0(\mathbf{L} - s) ds, \quad (2.3.2)$$

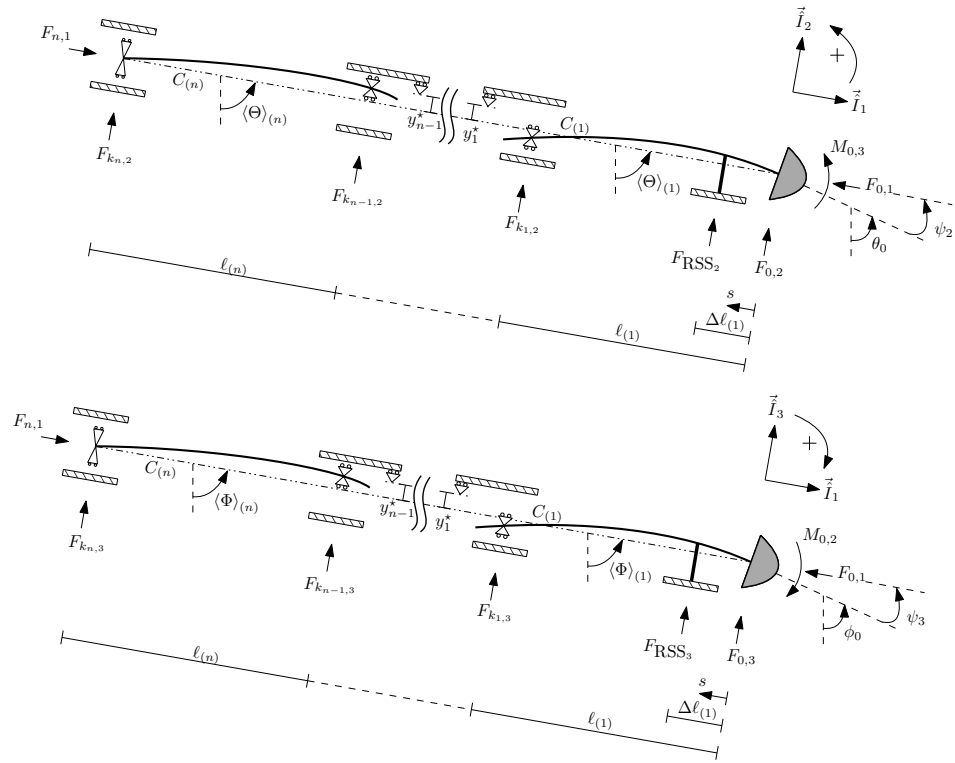


Figure 2.3.1: Schematic overview of a n-stabilizer BHA in both the (\vec{I}_1, \vec{I}_2) plane and the (\vec{I}_1, \vec{I}_3) . The forces and moments are included as well as some distances and inclinations.

$$\langle \Phi \rangle_{(i)}(\mathbf{L}) := \frac{1}{\ell_{(i)}} \int_{s_{i-1}}^{s_i} \Phi_0(\mathbf{L} - s) ds. \quad (2.3.3)$$

For the modeling of the BHA, an undeformed reference configuration is assumed, which implies that the chords $C_{(i)}$, for $i = 2, 3, \dots, n$, are aligned with the chord $C_{(1)}$. This is valid as long as the angle difference $\langle \Theta \rangle_{(1)} - \langle \Theta \rangle_{(i)}$ and $\langle \Phi \rangle_{(1)} - \langle \Phi \rangle_{(i)}$ is small. Consequently, all the lateral forces on the BHA are orthogonal to $\vec{\hat{I}}_1$, respectively. The axial forces are in line with the chord $C_{(1)}$, which is in the $\vec{\hat{I}}_1$ direction.

The RSS actuator is located at a distance $\Delta \ell_{(1)}$ from the bit where $\Delta \in (0, 1)$. The actuator force is defined as

$$\vec{F}_{RSS} = [F_{RSS,1} \quad F_{RSS,2} \quad F_{RSS,3}] \vec{\hat{I}} = \left(\underline{F}_{RSS}^{\hat{I}} \right)^{\top} \vec{\hat{I}}. \quad (2.3.4)$$

It is assumed that the actuator force is perpendicular to $\vec{\hat{I}}_1$, which implies that $F_{RSS,1} = 0$. As aforementioned, the last stabilizer is modeled as an ideal one which means that the stabilizer and the borehole have the same diameter and thus their centers must coincide. As a consequence, there is a wall contact force \vec{F}_n . In reality, the diameter of the stabilizer is smaller than the diameter of the borehole because of bit over-gauging and BHA whirling. This also implies that the stabilizers can move arbitrarily within the boundaries of the borehole. The stabilizers can either touch the wall at one point or not touch the wall at all. At each point s , the BHA has a certain deflection with respect to chord $C_{(1)}$. This deflection is a function of s along the BHA and of the borehole length \mathbf{L} , which is denoted by $\vec{h}(s, \mathbf{L})$. The variable \mathbf{L} is also the evolution variable. At the stabilizer positions, this deflection is evaluated at $s = s_i$ which is denoted as $\vec{h}_i = [h_{i,1} \quad h_{i,2} \quad h_{i,3}] \vec{\hat{I}} = \left(\underline{h}_i^{\hat{I}} \right)^{\top} \vec{\hat{I}}$. Since the position of the stabilizer along the curvilinear coordinate s does not change during borehole propagation, one can state that $h_{i,1} = 0$. A schematic representation of this scenario is given in Figure 2.3.2. At each stabilizer a lateral contact force \vec{F}_i is defined as

$$\vec{F}_i = [F_{i,1} \quad F_{i,2} \quad F_{i,3}] \vec{\hat{I}} = \left(\underline{F}_i^{\hat{I}} \right)^{\top} \vec{\hat{I}}, \quad (2.3.5)$$

which is also represented in Figure 2.3.2. The axial component $F_{i,1}$, for $i = 1, 2, \dots, n - 1$, is zero at each non-ideal stabilizer. At the ideal stabilizer at the end of the BHA, i.e., at $i = n$, the axial component represents the effect of the upper part of the drillstring on the BHA. Lastly, the force at the bit, $\vec{F}_0 = [-F_{0,1} \quad F_{0,2} \quad F_{0,3}] \vec{\hat{I}} = \left(\underline{F}_0^{\hat{I}} \right)^{\top} \vec{\hat{I}}$, and the moment at the bit, $\vec{M}_0 = [M_{0,1} \quad M_{0,2} \quad M_{0,3}] \vec{\hat{I}} = \left(\underline{M}_0^{\hat{I}} \right)^{\top} \vec{\hat{I}}$ are defined. For the BHA model, the forces are expressed in $\vec{\hat{I}}$, which should be taken into account when combining different components. The last force which is introduced is gravity acting on the BHA. This force acts

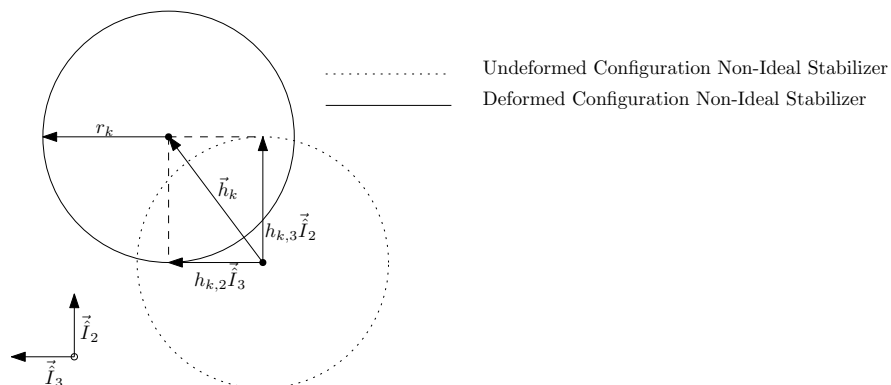


Figure 2.3.2: Schematic overview of the deformed BHA compared to an undeformed BHA at $s = s_k$. The difference in center points is represented by the vector \vec{h} , whilst r_k is the radius of the stabilizer.

in the \vec{e}_z direction of the earth-fixed frame, which means that the total weight is defined as $\vec{W} = w \sum_{k=1}^n \ell_{(k)} [\cos(\langle \Theta \rangle_{(1)}) \quad -\sin(\langle \Theta \rangle_{(1)}) \quad 0] = \left(\underline{W}^{\hat{I}} \right)^{\top} \vec{\underline{I}}$ where w is the distributed weight of the BHA. The angles $\langle \Theta \rangle_{(1)}$ and $\langle \Phi \rangle_{(1)}$ can be used since it is assumed that the BHA is aligned with chord $C_{(1)}$.

The BHA is split into $n + 1$ segments starting from the bit. The different segments correspond to shear force discontinuities and are indicated with $S_{(i)}$, for $i = 0, 1, \dots, n$, are defined as

$$S_{(i)} = \begin{cases} \{s \in [0, \Delta\ell_{(1)}]\} & \text{for } i = 0, \\ \{s \in [\Delta\ell_{(1)}, s_i]\} & \text{for } i = 1, \\ \{s \in [s_{i-1}, s_i]\} & \text{for } i = 2, 3, \dots, n. \end{cases} \quad (2.3.6)$$

Variables which have brackets around their index, for example the segment variable $S_{(i)}$, indicate that the variable corresponds to the segment instead of a separate point. Without those brackets, the variable refers to a specific stabilizer.

2.4 Model Components

The model to predict the propagation of the borehole consists of three interrelated components, as visualized in Figure 2.4.1. The complete model combines a BHA model, the bit-rock interface laws, and the bit kinematics. The bit kinematics relate the movement of the bit through the rock formation to the local geometry of the borehole. The bit-rock interface laws, relate this movement to the forces and moments which act on the bit. Then, the BHA model relates the forces and moments at the bit, as well as other external forces, to the deflection of the BHA. This deflection determines the bit orientation.

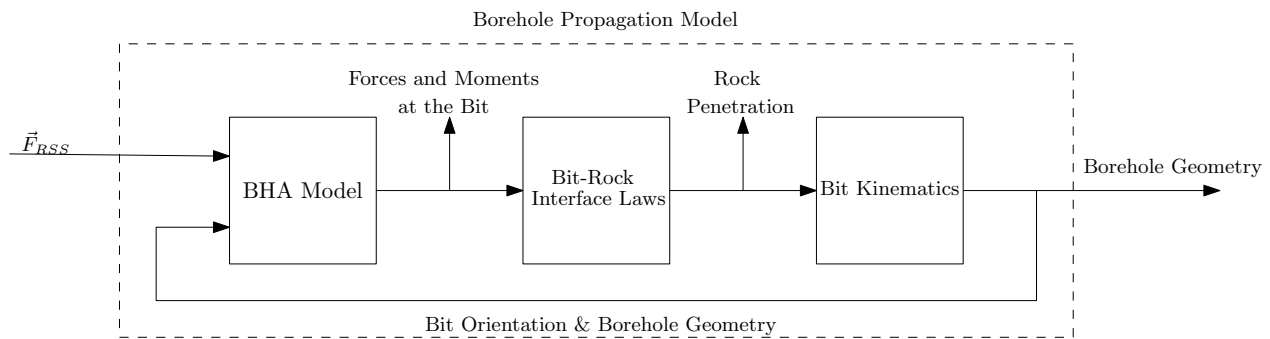


Figure 2.4.1: The interaction between the three model components of the borehole propagation model.

2.4.1 Kinematics

The kinematics of the bit are defined by its instantaneous velocity \vec{v} and spin $\vec{\omega}$. The rotation of the bit around the \vec{i}_1 axis is characterized by angular velocity vector $\vec{\Omega} = \Omega \vec{i}_1$. The penetration vector \vec{d} and angular penetration $\vec{\varphi}$ are defined as

$$\vec{d} = \frac{2\pi\vec{v}}{\Omega} \quad \text{and} \quad \vec{\varphi} = \frac{2\pi\vec{\omega}}{\Omega}. \quad (2.4.1)$$

These vectors can be decomposed in the reference frame \vec{i} into axial penetration d_1 , lateral penetrations d_2 and d_3 and angular penetrations φ_2 and φ_3 when projected on the system axes \vec{i}_1 . The penetration vector \vec{d} defines the drilling direction at the bit, thus $\vec{d} = d\vec{I}_1$ where $d = \sqrt{d_1^2 + d_2^2 + d_3^2}$, i.e., \vec{d} is in the direction along which the borehole evolves. Angular penetration $\vec{\varphi}$ defines the instantaneous change of orientation of the bit. Both \vec{d} and $\vec{\varphi}$ are velocities that measure bit propagation per revolution of the bit.

The bit tilt angles are defined by the relative orientation of \vec{I}_1 with respect to the bit axis \vec{i}_1 . Since \vec{d} is aligned with \vec{I}_1 , the bit tilt angles can be expressed in terms of \vec{d} . The bit tilt angles correspond to the relative inclinations of the projection of \vec{d} in the planes (\vec{i}_1, \vec{i}_2) and (\vec{i}_2, \vec{i}_3) . The angles are measured from the projection of \vec{d} to \vec{i}_1 around, respectively, $-\vec{i}_3$ and \vec{i}_2 . Calculating the inclination angle of the projection leads to the bit tilt angles

$$\psi_2 = -\arctan\left(\frac{d_2}{d_1}\right) \approx -\frac{d_2}{d_1}, \quad \text{and} \quad \psi_3 = -\arctan\left(\frac{d_3}{d_1}\right) \approx -\frac{d_3}{d_1}, \quad (2.4.2)$$

where the small angle approximation $\arctan(\alpha) \approx \alpha$ is used. This is valid since $d_1 \gg d_2$ and $d_1 \gg d_3$ as bits are designed to drill dominantly in the axial direction. By using $\vec{d} = [d_1 \ d_2 \ d_3] \vec{i} \approx d\vec{I}_1$ and the expression $\vec{I} = \underline{A}_{Ii}(\Phi, \phi, \Theta, \theta) \vec{i}$, where

$$\underline{A}_{Ii}(\Phi, \phi, \Theta, \theta) = \underline{A}_I(\Phi, \Theta) \underline{A}_i(\phi, \theta)^\top = \begin{bmatrix} s_\Theta s_\theta c_{\phi-\Phi} + c_\theta c_\Theta & c_\theta s_\Theta c_{\phi-\Phi} - s_\theta c_\Theta & -s_\Theta s_{\phi-\Phi} \\ c_\Theta s_\theta c_{\phi-\Phi} - c_\theta s_\Theta & c_\theta c_\Theta c_{\phi-\Phi} + s_\theta s_\Theta & -c_\Theta s_{\phi-\Phi} \\ s_\theta s_{\phi-\Phi} & c_\theta s_{\phi-\Phi} & c_{\phi-\Phi} \end{bmatrix}, \quad (2.4.3)$$

the bit tilt angles can be expressed in terms of \vec{i} as

$$\begin{aligned}\psi_2 &\approx -\frac{d_2}{d_1} \approx -\frac{c_\theta s_\Theta c_{\phi-\Phi} - s_\theta c_\Theta}{s_\Theta s_\theta c_{\phi-\Phi} + c_\theta c_\Theta} \approx \frac{s_{\theta-\Theta}}{c_{\theta-\Theta}} \approx \theta - \Theta, \\ \psi_3 &\approx -\frac{d_3}{d_1} \approx \frac{-s_\Theta s_{\phi-\Phi}}{s_\Theta s_\theta c_{\phi-\Phi} + c_\theta c_\Theta} \approx \frac{s_\Theta s_{\phi-\Phi}}{c_{\theta-\Theta}} \approx s_\Theta(\phi - \Phi),\end{aligned}\tag{2.4.4}$$

where the facts $|\theta - \Theta| \ll 1$ and $|\phi - \Phi| \ll 1$ have been applied to do the approximations, stemming from the fact that the bit axis \mathcal{D} is a small perturbation of the borehole axis \mathcal{B} . In conclusion, (2.4.4) relates the penetration variables and the bit tilt in terms of the bit and borehole inclination and azimuth. The change of inclination and azimuth at the bit can be computed by using (2.4.1) and the definition of the spin vector $\vec{\omega} = \left[0 \quad -\frac{d\phi}{dt} \sin \theta \quad \frac{d\theta}{dt}\right] \vec{i}$ such that

$$\begin{bmatrix} 0 & \varphi_2 & \varphi_3 \end{bmatrix} \vec{i} = \frac{2\pi}{\Omega} \begin{bmatrix} 0 & -\frac{d\phi}{dt} \sin \theta & \frac{d\theta}{dt} \end{bmatrix} \vec{i} = \frac{2\pi}{\Omega} \begin{bmatrix} 0 & -\frac{d\phi}{dL} \frac{dL}{dt} \sin \theta & \frac{d\theta}{dL} \frac{dL}{dt} \end{bmatrix} \vec{i},\tag{2.4.5}$$

which, by using $\frac{dL}{dt} = \|\vec{v}\|$, leads to

$$\frac{\varphi_2}{d_1} \approx -\frac{d\phi}{dL} \sin \theta, \quad \text{and} \quad \frac{\varphi_3}{d_1} \approx \frac{d\theta}{dL},\tag{2.4.6}$$

where there is used that d_1 is the time derivative of the borehole length, i.e., $d_1 = \frac{dL}{dt}$.

2.4.2 Bit/rock Interface Laws

The interface laws are represented with respect to one reference point on the bit. This reference point is located at the lower boundary of the BHA model along \vec{i}_1 . The bit/rock interaction forces are reduced to generalized forces averaged over a bit revolution, namely a force acting on the bit and moment acting at the reference point on the bit and being orthogonal to the bit axis \vec{i}_1 . The force at the bit is defined as $\vec{\hat{F}}_0 = \begin{bmatrix} -\hat{F}_{0,1} & \hat{F}_{0,2} & \hat{F}_{0,3} \end{bmatrix} \vec{i} = \left(\hat{F}_0^i\right)^\top \vec{i}$ and the moment at the bit location is defined as $\vec{\hat{M}}_0 = \begin{bmatrix} \hat{M}_{0,1} & \hat{M}_{0,2} & \hat{M}_{0,3} \end{bmatrix} \vec{i} = \left(\hat{M}_0^i\right)^\top \vec{i}$. The forces and moments acting on the bit are related to the penetration vector \vec{d} and angular penetration vector $\vec{\varphi}$ by the bit/rock interface laws [23], which can be expressed as follows:

$$\begin{Bmatrix} \hat{F}_{0,1} \\ \hat{F}_{0,2} \\ \hat{F}_{0,3} \\ \hat{M}_{0,2} \\ \hat{M}_{0,3} \end{Bmatrix} = - \begin{Bmatrix} G_1 \\ 0 \\ 0 \\ 0 \\ 0 \end{Bmatrix} - \begin{bmatrix} H_1 & 0 & 0 & 0 & 0 \\ 0 & H_2 & H_3 & 0 & 0 \\ 0 & -H_3 & H_2 & 0 & 0 \\ 0 & 0 & 0 & H_4 & H_5 \\ 0 & 0 & 0 & -H_5 & H_4 \end{bmatrix} \begin{Bmatrix} d_1 \\ d_2 \\ d_3 \\ \varphi_2 \\ \varphi_3 \end{Bmatrix}.\tag{2.4.7}$$

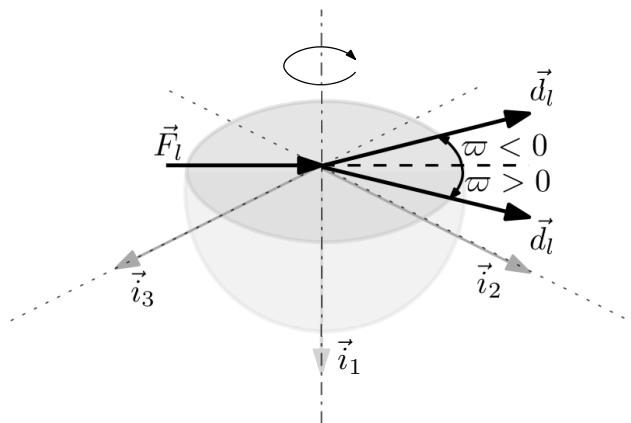


Figure 2.4.2: Visualisation of the bit walk angle, adopted from [15].

The term G_1 is a measure for the bluntness of the bit and is always positive. The coefficients H_i , for $i = 1, 2, \dots, 5$, depend on the bit geometry, the rock strength and parameters of the bit itself. The parameters H_i , for $i = 1, 2, \dots, 5$, could be interpreted as damping coefficients. A walk angle ϖ is defined as the difference in angle between the lateral penetration d_2 and d_3 and the lateral force F_2 and F_3 and is defined as follows

$$\varpi := \arctan \frac{H_3}{H_2}. \quad (2.4.8)$$

If $\varpi = 0$, the lateral forces and penetrations are aligned, which causes the bit to have a neutral walk tendency. If $\varpi > 0$ the bit has a right walk-tendency, whilst $\varpi < 0$ implies the bit has a left-walk-tendency. For PDC bits, walk angles of $\pm 10^\circ$ are not uncommon [15]. The bit walk is visualized in Figure 2.4.2. The bit walk angle is the angle between the lateral penetration, defined as $\vec{d}_l := d_2 \vec{i}_2 + d_3 \vec{i}_3$, and the lateral forces, defined as $\vec{F}_l := \hat{F}_{0,2} \vec{i}_2 + \hat{F}_{0,3} \vec{i}_3$ pointing in the direction of \vec{i}_1 . Besides the bit walk, also bit flip ς is defined. This ς , analog to the bit walk, is the difference in orientation between the moments at the bit $\vec{M}_b = M_2 \vec{i}_2 + M_3 \vec{i}_3$ and the change of bit orientation $\vec{\varphi}_b = \varphi_2 \vec{i}_2 + \varphi_3 \vec{i}_3$. In terms of H_4 and H_5 , the bit flip is defined as

$$\varsigma := \arctan \frac{H_5}{H_4}. \quad (2.4.9)$$

The active weight on the bit W can be derived from the first equation of (2.4.7) and is $W = H_1 d_1 = -G_1 - \hat{F}_{0,1}$.

Next, the bit/rock interface laws (2.4.7), the definition of the active weight W and the

kinematic relations (2.4.4), (2.4.6) are combined to derive

$$\begin{bmatrix} \hat{F}_{0,2} \\ \hat{F}_{0,3} \end{bmatrix} = d_1 \begin{bmatrix} H_2 & H_3 \\ -H_3 & H_2 \end{bmatrix} \begin{bmatrix} \varphi_2 \\ \varphi_3 \end{bmatrix} = W \begin{bmatrix} \frac{H_2}{H_1} & \frac{H_3}{H_1} \\ -\frac{H_3}{H_1} & \frac{H_2}{H_1} \end{bmatrix} \begin{bmatrix} \psi_2 \\ \psi_3 \end{bmatrix}, \quad (2.4.10)$$

$$\begin{bmatrix} \hat{M}_{0,2} \\ \hat{M}_{0,3} \end{bmatrix} = d_1 \begin{bmatrix} H_4 & -H_5 \\ -H_5 & -H_4 \end{bmatrix} \begin{bmatrix} \frac{d\phi}{dL} \sin(\theta) \\ \frac{d\theta}{dL} \end{bmatrix} = W \begin{bmatrix} \frac{H_4}{H_1} & -\frac{H_5}{H_1} \\ -\frac{H_5}{H_1} & -\frac{H_4}{H_1} \end{bmatrix} \begin{bmatrix} \frac{d\phi}{dL} \sin(\theta) \\ \frac{d\theta}{dL} \end{bmatrix}. \quad (2.4.11)$$

2.4.3 Scaling of Variables

To generalize the modeling and analysis of the borehole propagation model, scaling of the variables is introduced. Both the forces and moments, as well as the lengths are scaled. To scale the length, the reference length $\ell_{(1)}$ is used. Using this scale, a couple of different dimensionless parameters are introduced. The first is $\lambda_{(i)}$, for $i = 1, 2, \dots, n$, which is defined as $\lambda_{(i)} := \ell_{(i)}/\ell_{(1)}$. This parameters indicates the distance between two consecutive stabilizers. This definition implies that $\lambda_{(1)} = 1$. The dimensionless total length of the BHA is defined as $\lambda := \sum_{k=1}^n \lambda_{(k)}$. Secondly, the dimensionless total borehole length ξ is defined as $\xi := \frac{L}{\ell_{(1)}}$. Thirdly, the arc length along the BHA starting from the bit is defined as $\tilde{s} := \frac{s}{\ell_{(1)}}$ on which the stabilizer positions are defined as $\tilde{s}_i := \frac{s_i}{\ell_{(1)}}$. Using these scaled parameters, the segments of the BHA can be written as

$$\tilde{S}_{(i)} = \begin{cases} \{\tilde{s} \in [0, \Delta]\} & \text{for } i = 0, \\ \{\tilde{s} \in [\Delta, 1]\} & \text{for } i = 1, \\ \{\tilde{s} \in [\tilde{s}_{i-1}, \tilde{s}_i]\} & \text{for } i = 2, 3, \dots, n. \end{cases} \quad (2.4.12)$$

The deflection of the stabilizers, denoted by \vec{h}_i , is scaled to be $\vec{h}_i := \frac{\vec{h}}{\ell_{(1)}} = [\tilde{h}_{i,1} \quad \tilde{h}_{i,2} \quad \tilde{h}_{i,3}] \vec{\underline{I}} = \left(\begin{smallmatrix} \tilde{h}_i \\ \tilde{h}_i \end{smallmatrix} \right)^\top \vec{\underline{I}}$.

To scale the forces and moments, the characteristic force $F^* := 3\frac{EI}{\ell_{(1)}^2}$ is defined, where EI is the flexural stiffness. With this characteristic force, several dimensionless forces are defined. The first scaled force is the force at the bit, which is scaled to be $\vec{F}_0 = \frac{\vec{F}_0}{F^*} = [-\tilde{F}_{0,1} \quad \tilde{F}_{0,2} \quad \tilde{F}_{0,3}] \vec{\underline{I}} = \left(\begin{smallmatrix} \tilde{F}_0 \\ \tilde{F}_0 \end{smallmatrix} \right)^\top \vec{\underline{I}}$. Similarly, the contact forces are defined as $\vec{F}_k = \frac{\vec{F}_k}{F^*} = [\tilde{F}_d \quad \tilde{F}_{k,2} \quad \tilde{F}_{k,3}] \vec{\underline{I}} = \left(\begin{smallmatrix} \tilde{F}_k \\ \tilde{F}_k \end{smallmatrix} \right)^\top \vec{\underline{I}}$. The actuator force is scaled to be $\vec{F}_{RSS} = \frac{\vec{F}_{RSS}}{F^*} = [\tilde{F}_{RSS,1} \quad \tilde{F}_{RSS,2} \quad \tilde{F}_{RSS,3}] \vec{\underline{I}} = \left(\begin{smallmatrix} \tilde{F}_{RSS} \\ \tilde{F}_{RSS} \end{smallmatrix} \right)^\top \vec{\underline{I}}$. Lastly, the distributed weight of the BHA is scaled to be $\tilde{w} = w \frac{\ell_{(1)}}{F^*}$. To scale the moment at the bit, the characteristic moment $M^* = F^* \ell_{(1)}$ is defined leading to $\vec{M}_0 = \frac{\vec{M}_0}{M^*} = [\tilde{M}_{0,1} \quad \tilde{M}_{0,2} \quad \tilde{M}_{0,3}] = \left(\begin{smallmatrix} \tilde{M}_0 \\ \tilde{M}_0 \end{smallmatrix} \right)^\top \vec{\underline{I}}$. These definitions

can be applied to obtain the scaled version of (2.4.10)

$$\begin{bmatrix} \tilde{F}_{0,2} \\ \tilde{F}_{0,3} \end{bmatrix} = \begin{bmatrix} \hat{F}_{0,2} \\ \hat{F}_{0,3} \\ F^* \end{bmatrix} = \frac{W}{F^*} \frac{\sqrt{H_2^2 + H_3^2}}{H_1} \begin{bmatrix} \frac{H_2}{\sqrt{H_2^2 + H_3^2}} & \frac{H_3}{\sqrt{H_2^2 + H_3^2}} \\ -\frac{H_3}{\sqrt{H_2^2 + H_3^2}} & \frac{H_2}{\sqrt{H_2^2 + H_3^2}} \end{bmatrix} \begin{bmatrix} \psi_2 \\ \psi_3 \end{bmatrix} = \Pi \eta \begin{bmatrix} \cos(\varpi) & \sin(\varpi) \\ -\sin(\varpi) & \cos(\varpi) \end{bmatrix} \begin{bmatrix} \psi_2 \\ \psi_3 \end{bmatrix}, \quad (2.4.13)$$

where the scaled active weight on the bit is defined as $\Pi := \frac{W}{F^*}$ and the lateral steering resistance $\eta := \frac{\sqrt{H_2^2 + H_3^2}}{H_1}$ is introduced. This steering resistance η is a positive number which indicates the difficulty of lateral penetration in comparison to axial penetration. Scaling can also be applied to the equation of the moments in (2.4.11) leading to

$$\begin{aligned} \begin{bmatrix} \tilde{M}_{0,2} \\ \tilde{M}_{0,3} \end{bmatrix} &= \begin{bmatrix} \hat{M}_{0,2} \\ M^* \\ \hat{M}_{0,3} \\ M^* \end{bmatrix} = \frac{W}{F^*} \frac{\sqrt{H_4^2 + H_5^2}}{H_1 \ell_{(1)}} \begin{bmatrix} \frac{H_4}{\sqrt{H_4^2 + H_5^2}} & -\frac{H_5}{\sqrt{H_4^2 + H_5^2}} \\ -\frac{H_5}{\sqrt{H_4^2 + H_5^2}} & \frac{H_4}{\sqrt{H_4^2 + H_5^2}} \end{bmatrix} \begin{bmatrix} \frac{d\phi}{dL} \sin(\theta) \\ \frac{d\theta}{dL} \end{bmatrix} \\ &= -\Pi \chi \begin{bmatrix} -\cos(\varsigma) & \sin(\varsigma) \\ \sin(\varsigma) & \cos(\varsigma) \end{bmatrix} \begin{bmatrix} \frac{d\phi}{d\xi} \sin(\theta) \\ \frac{d\theta}{d\xi} \end{bmatrix}. \end{aligned} \quad (2.4.14)$$

In this equation, the angular steering resistance $\chi := \frac{\sqrt{H_4^2 + H_5^2}}{H_1 \ell_{(1)}}$ is introduced. This steering resistance is a positive number which measures the relative difficulty of imposing an angular penetration.

2.5 BHA Model Derivation

The BHA model relates the deflection of the BHA to the forces and moments which act on it, given that the bit and borehole orientations are known. The BHA can be modeled as a static beam which is supported at the bit and submitted to contact forces at the stabilizers and RSS actuator. Therefore, the static equilibrium equations

$$\sum \vec{F} = \vec{0}, \sum \vec{M} = \vec{0} \quad (2.5.1)$$

must hold. The forces and moments, however, are statically indeterminate; i.e., the deformation of the BHA should be considered to determine the forces and moments acting on the BHA.

For an n -stabilizer BHA, the equilibrium equations (2.5.1) are derived based on Figure 2.3.1

and are given as follows:

$$\begin{aligned} \sum \vec{F} &= \left(\vec{F}_0 + \vec{F}_{RSS} + \sum_{k=1}^{n-1} \vec{F}_k + \vec{F}_n + \underline{W} \right) \vec{I} \\ &= \begin{bmatrix} -\vec{F}_{0,1} + \vec{F}_d + \tilde{w} \lambda \cos \langle \Theta \rangle_{(1)} \\ \vec{F}_{0,2} + \vec{F}_{RSS,2} + \sum_{k=1}^n \vec{F}_{k,2} - \tilde{w} \lambda \sin \langle \Theta \rangle_{(1)} \\ \vec{F}_{0,3} + \vec{F}_{RSS,3} + \sum_{k=1}^n \vec{F}_{k,3} \end{bmatrix} \vec{I} = \vec{0}, \end{aligned} \quad (2.5.2)$$

$$\begin{aligned} \sum \vec{M}_{w.r.t.bit} &= \underline{M}_0 \vec{I} - \underline{M}_n \vec{I} + \begin{bmatrix} -\Delta \\ 0 \\ 0 \end{bmatrix}^\top \vec{I} \times (\vec{F}_{RSS} \vec{I})^\top + \sum_{k=1}^n \begin{bmatrix} -\tilde{s}_k \\ 0 \\ 0 \end{bmatrix}^\top \vec{I} \times (\vec{F}_k \vec{I})^\top + \begin{bmatrix} -\frac{\lambda}{2} \\ 0 \\ 0 \end{bmatrix}^\top \vec{I} \times (\underline{W} \vec{I})^\top \\ &= \begin{bmatrix} -\tilde{M}_{n,1} + \tilde{M}_{0,1} \\ \tilde{M}_{0,2} + \Delta \vec{F}_{RSS,3} + \sum_{k=1}^n \tilde{s}_k \vec{F}_{k,3} \\ \tilde{M}_{0,3} - \Delta \vec{F}_{RSS,2} - \sum_{k=1}^n \tilde{s}_k \vec{F}_{k,2} + \frac{1}{2} \tilde{w} \lambda^2 \sin \langle \Theta \rangle_{(1)} \end{bmatrix} \vec{I} = \vec{0}. \end{aligned} \quad (2.5.3)$$

The deflection at stabilizers $i = 1, 2, \dots, n-1$, earlier defined as \vec{h}_i , is the distance between the chord $C_{(1)}$ and the BHA at the position of stabilizer i . This deflection corresponds to an angle, the angle between chord $C_{(1)}$ and the tangent to the BHA axis at $s = s_k$, defined as $\mathcal{H}_j(\tilde{s}, \mathbf{L})$, for $j \in [2, 3]$. Angle $\mathcal{H}_3(\tilde{s}, \mathbf{L})$ corresponds to the angle between chord $C_{(1)}$ and the tangent to the BHA in the (\vec{I}_1, \vec{I}_2) plane and angle $\mathcal{H}_2(\tilde{s}, \mathbf{L})$ corresponds to the angle between chord $C_{(1)}$ and the tangent to the BHA in the (\vec{I}_1, \vec{I}_3) plane. The deflection and its corresponding angle can be used to solve the scaled Euler-Bernoulli equation

$$3\tilde{M}_2 = -\frac{d^2 \tilde{h}_3(\tilde{s}, \mathbf{L})}{d\tilde{s}^2} = -\frac{d\mathcal{H}_2(\tilde{s}, \mathbf{L})}{d\tilde{s}}, \quad 3\tilde{M}_3 = \frac{d^2 \tilde{h}_2(\tilde{s}, \mathbf{L})}{d\tilde{s}} = \frac{d\mathcal{H}_3(\tilde{s}, \mathbf{L})}{d\tilde{s}}, \quad (2.5.4)$$

where the relations

$$\mathcal{H}_2(\tilde{s}, \mathbf{L}) = \frac{d\tilde{h}_3(\tilde{s}, \mathbf{L})}{d\tilde{s}}, \quad \mathcal{H}_3(\tilde{s}, \mathbf{L}) = \frac{d\tilde{h}_2(\tilde{s}, \mathbf{L})}{d\tilde{s}}, \quad (2.5.5)$$

are applied.

The relative inclinations and azimuths, $\mathcal{H}_2(\tilde{s}, \mathbf{L})$ and $\mathcal{H}_3(\tilde{s}, \mathbf{L})$, are determined by integrating the Euler-Bernoulli equations. The first step in solving the equation is to obtain an expression for the internal moment in the BHA, which is obtained by the method of intersections [11]. The internal moment is defined as $\vec{M}_{(i)}(s) = \begin{bmatrix} \tilde{M}_{(i),1} & \tilde{M}_{(i),2} & \tilde{M}_{(i),3} \end{bmatrix} \vec{I} = \underline{M}_{(i)} \vec{I}$, for $i = 0, 1, \dots, n$. First, the moment equilibrium is defined for section $S_{(n)}$, followed by the

moment equilibrium for section $S_{(n-1)}$. This process continues up to $S_{(0)}$, leading to

$$\tilde{M}_{(i)}(\tilde{s}) = \begin{cases} \begin{bmatrix} \star \\ \tilde{M}_{(i+1,2)} \\ \tilde{M}_{(i+1,3)} \end{bmatrix} + (\Delta - \tilde{s}) \begin{bmatrix} \star \\ -\tilde{F}_{RSS,3} \\ \tilde{F}_{RSS,2} \end{bmatrix} & \text{for } i = 0, \\ \begin{bmatrix} \star \\ \tilde{M}_{(i+1,2)} \\ \tilde{M}_{(i+1,3)} \end{bmatrix} + (\tilde{s}_i - \tilde{s}) \begin{bmatrix} \star \\ -\tilde{F}_{i,3} \\ \tilde{F}_{i,2} \end{bmatrix} & \text{for } i = 1, 2, \dots, n-1, \\ (\lambda - \tilde{s}) \begin{bmatrix} \star \\ -\tilde{F}_{i,3} \\ \tilde{F}_{i,2} \end{bmatrix} - \begin{bmatrix} \star \\ 0 \\ \frac{1}{2}\tilde{w}(\lambda - \tilde{s})^2 \sin \langle \Theta \rangle_{(1)} \end{bmatrix} & \text{for } i = n. \end{cases} \quad (2.5.6)$$

The internal moments in the direction of $\vec{\hat{I}}_1$ are indicated with a \star because these are irrelevant for the deflection of the BHA in the $\vec{\hat{I}}_2$ and $\vec{\hat{I}}_3$ direction. Using the relation (2.5.4), the relative inclination $\mathcal{H}_{(i)}(\tilde{s}) = [\star \quad \mathcal{H}_{(i,2)} \quad \mathcal{H}_{(i,3)}] \vec{\hat{I}}$ and the deflection $\tilde{h}_{(i)}(\tilde{s}) = [\star \quad \tilde{h}_{(i,2)} \quad \tilde{h}_{(i,3)}] \vec{\hat{I}}$ with respect to the chord C_1 can be found per segment (i) by integration:

$$\begin{aligned} \mathcal{H}_{(i)}(\tilde{s}) &= 3 \int_0^{\tilde{s}} \tilde{M}_{(i)}(\tau) d\tau + \bar{\mathcal{H}}_i \quad \text{for } \tilde{s} \in \tilde{S}_{(i)}, \\ \tilde{h}_{(i)}(\tilde{s}) &= \int_0^{\tilde{s}} \mathcal{H}_{(i)}(\tau) d\tau + \bar{h}_i \quad \text{for } \tilde{s} \in \tilde{S}_{(i)}, \end{aligned} \quad (2.5.7)$$

for $i = 0, 1, \dots, n$, and with the integration constants $\bar{\mathcal{H}}_i$ and \bar{h}_i , which leads to

$$\mathcal{H}_{(i)}(\tilde{s}) = \begin{cases} \begin{bmatrix} \star \\ \mathcal{H}_{(1,2)} \\ \mathcal{H}_{(1,3)} \end{bmatrix} (\tilde{s}) + 3(\Delta\tilde{s} - \frac{\tilde{s}^2}{2}) \begin{bmatrix} \star \\ \tilde{F}_{RSS,3} \\ \tilde{F}_{RSS,2} \end{bmatrix} + \begin{bmatrix} \star \\ \bar{\mathcal{H}}_{(0,2)} \\ \bar{\mathcal{H}}_{(0,3)} \end{bmatrix} & \text{for } i = 0, \\ \begin{bmatrix} \star \\ \mathcal{H}_{(i+1,2)} \\ \mathcal{H}_{(i+1,3)} \end{bmatrix} (\tilde{s}) + 3(\tilde{s}\tilde{s}_i - \frac{\tilde{s}^2}{2}) \begin{bmatrix} \star \\ \tilde{F}_{i,3} \\ \tilde{F}_{i,2} \end{bmatrix} + \begin{bmatrix} \star \\ \bar{\mathcal{H}}_{(i,2)} \\ \bar{\mathcal{H}}_{(i,3)} \end{bmatrix} & \text{for } i = 1, 2, \dots, n-1, \\ 3(\lambda\tilde{s} - \frac{\tilde{s}^2}{2}) \begin{bmatrix} \star \\ \tilde{F}_{n,3} \\ \tilde{F}_{n,2} \end{bmatrix} - \begin{bmatrix} \star \\ 0 \\ \frac{3}{2}\tilde{w}(\lambda^2\tilde{s} - \lambda\tilde{s}^2 + \frac{1}{3}\tilde{s}^3) \sin(\langle \Theta \rangle_{(1)}) \end{bmatrix} + \begin{bmatrix} \star \\ \bar{\mathcal{H}}_{(n,2)} \\ \bar{\mathcal{H}}_{(n,3)} \end{bmatrix} & \text{for } i = n, \end{cases} \quad (2.5.8)$$

for the relative inclination $\mathcal{H}_{\tilde{s},3}(\tilde{s})$ and azimuth $\mathcal{H}_{\tilde{s},2}(\tilde{s})$. From this, an expression for the relative deflection can be computed by integration:

$$\tilde{h}_{(i)}(\tilde{s}) = \begin{cases} \begin{bmatrix} \star \\ \tilde{h}_{(1,2)} \\ \tilde{h}_{(1,3)} \end{bmatrix} (\tilde{s}) + (\frac{3}{2}\Delta\tilde{s}^2 - \frac{\tilde{s}^3}{2}) \begin{bmatrix} \star \\ \tilde{F}_{RSS,2} \\ \tilde{F}_{RSS,3} \end{bmatrix} + \begin{bmatrix} \star \\ \bar{\mathcal{H}}_{(0,3)} \\ \bar{\mathcal{H}}_{(0,2)} \end{bmatrix} \tilde{s} + \begin{bmatrix} \star \\ \bar{h}_{(0,2)} \\ \bar{h}_{(0,3)} \end{bmatrix} & \text{for } i = 0, \\ \begin{bmatrix} \star \\ \tilde{h}_{(i+1,2)} \\ \tilde{h}_{(i+1,3)} \end{bmatrix} (\tilde{s}) + (\frac{3\tilde{s}^2\tilde{s}_i}{2} - \frac{\tilde{s}^3}{2}) \begin{bmatrix} \star \\ \tilde{F}_{i,2} \\ \tilde{F}_{i,3} \end{bmatrix} + \begin{bmatrix} \star \\ \bar{\mathcal{H}}_{(i,3)} \\ \bar{\mathcal{H}}_{(i,2)} \end{bmatrix} \tilde{s} + \begin{bmatrix} \star \\ \bar{h}_{(i,2)} \\ \bar{h}_{(i,3)} \end{bmatrix} & \text{for } i = 1, 2, \dots, n-1, \\ \frac{3}{2}(\lambda\tilde{s}^2 - \frac{\tilde{s}^3}{3}) \begin{bmatrix} \star \\ \tilde{F}_{n,2} \\ \tilde{F}_{n,3} \end{bmatrix} - \begin{bmatrix} \star \\ \frac{3}{2}\tilde{w}(\frac{\lambda^2\tilde{s}^2}{2} - \frac{\lambda\tilde{s}^3}{3} + \frac{\tilde{s}^4}{12}) \sin(\langle \Theta \rangle_{(1)}) \\ 0 \end{bmatrix} + \begin{bmatrix} \star \\ \bar{\mathcal{H}}_{(n,3)} \\ \bar{\mathcal{H}}_{(n,2)} \end{bmatrix} \tilde{s} + \begin{bmatrix} \star \\ \bar{h}_{(n,2)} \\ \bar{h}_{(n,3)} \end{bmatrix} & \text{for } i = n. \end{cases} \quad (2.5.9)$$

One should be aware that these deflections and relative inclinations are only valid when evaluated in the corresponding segment, thus $\tilde{s} \in \tilde{S}_{(i)}$. The number of unknowns in this problem is $8n + 9$. These unknowns consists of three forces $\left(\underline{F}_0^{\hat{i}}\right)^\top \tilde{\underline{I}}$, as well as three moments $\left(\underline{M}_0^{\hat{i}}\right)^\top \tilde{\underline{I}}$, at the bit. These unknowns can be obtained from the static equilibrium equations, which were derived earlier in equations (2.5.2) and (2.5.3) under the assumptions that the moments and axial force at the last stabilizer are known. The next three unknowns are the contact forces at the last ideal stabilizer $\left(\underline{F}_n^{\hat{i}}\right)^\top \tilde{\underline{I}}$, which follow from the deflection at the last stabilizer. For the $n - 1$ non-ideal stabilizers, a nonlinear complementarity problem, which is treated later on, is formulated to solve for these $4(n - 1)$ unknowns. The remaining $4(n + 1)$ unknowns are the integration constants $\bar{\mathcal{H}}_i$ and \bar{h}_i for $i = 1, 2, \dots, n$, which can be found by imposing continuity of the beam, bit centering, and the relation between the average angles $\langle \Theta \rangle_{(1)}$ and $\langle \Phi \rangle_{(1)}$ and the relative angles formulated in (2.5.8). The aim of imposing these constraints is to find an expression in closed form for the deflection of the BHA at its segments.

The first constraint is to impose that the relative inclination and azimuth are continuous along the BHA. At the RSS locations $\tilde{s} = \Delta$ and at each stabilizer positions $\tilde{s} = \tilde{s}_k$, it holds that

$$\begin{bmatrix} \mathcal{H}_{(1,2)} \\ \mathcal{H}_{(1,3)} \end{bmatrix} (\Delta) = \begin{bmatrix} \mathcal{H}_{(0,2)} \\ \mathcal{H}_{(0,3)} \end{bmatrix} (\Delta), \quad (2.5.10a)$$

$$\begin{bmatrix} \mathcal{H}_{(i+1,2)} \\ \mathcal{H}_{(i+1,3)} \end{bmatrix} (\tilde{s}_i) = \begin{bmatrix} \mathcal{H}_{(i,2)} \\ \mathcal{H}_{(i,3)} \end{bmatrix} (\tilde{s}_i) \text{ for } i = 1, 2, \dots, n - 1. \quad (2.5.10b)$$

Constraint (2.5.10a) leads to

$$\begin{bmatrix} \bar{\mathcal{H}}_{(1,2)} \\ \bar{\mathcal{H}}_{(1,3)} \end{bmatrix} = \frac{3}{2} \Delta^2 \begin{bmatrix} \tilde{F}_{RSS,3} \\ \tilde{F}_{RSS,2} \end{bmatrix}, \quad (2.5.11)$$

and for $i = 1, 2, \dots, n - 1$, the constraint (2.5.10b) leads to

$$\begin{bmatrix} \bar{\mathcal{H}}_{(i,2)} \\ \bar{\mathcal{H}}_{(i,3)} \end{bmatrix} = -\frac{3}{2} \tilde{s}_i^2 \begin{bmatrix} \tilde{F}_{i,3} \\ \tilde{F}_{i,2} \end{bmatrix}. \quad (2.5.12)$$

A similar continuity constraint can be imposed on the deflection, which is expressed as follows:

$$\begin{bmatrix} \tilde{h}_{(1,2)} \\ \tilde{h}_{(1,3)} \end{bmatrix} (\Delta) = \begin{bmatrix} \tilde{h}_{(0,2)} \\ \tilde{h}_{(0,3)} \end{bmatrix} (\Delta), \quad (2.5.13a)$$

$$\begin{bmatrix} \tilde{h}_{(i+1,2)} \\ \tilde{h}_{(i+1,3)} \end{bmatrix} (\tilde{s}_i) = \begin{bmatrix} \tilde{h}_{(i,2)} \\ \tilde{h}_{(i,3)} \end{bmatrix} (\tilde{s}_i) \text{ for } i = 1, 2, \dots, n - 1. \quad (2.5.13b)$$

Constraint (2.5.13a) leads to

$$\begin{bmatrix} \bar{h}_{(1,2)} \\ \bar{h}_{(1,3)} \end{bmatrix} = \frac{1}{2} \Delta^3 \begin{bmatrix} \tilde{F}_{RSS,2} \\ \tilde{F}_{RSS,3} \end{bmatrix}, \quad (2.5.14)$$

and for $i = 1, 2, \dots, n-1$, the constraint (2.5.13b) leads to

$$\begin{bmatrix} \bar{h}_{(i,2)} \\ \bar{h}_{(i,3)} \end{bmatrix} = \frac{1}{2} \tilde{s}_i^3 \begin{bmatrix} \tilde{F}_{i,2} \\ \tilde{F}_{i,3} \end{bmatrix}. \quad (2.5.15)$$

The next constraint which is considered is the fact that the bit is centered in the borehole and thus the deflection should be zero, i.e,

$$\begin{bmatrix} \tilde{h}_{(0,2)} \\ \tilde{h}_{(0,3)} \end{bmatrix} (0) = \begin{bmatrix} 0 \\ 0 \end{bmatrix}. \quad (2.5.16)$$

which results in

$$\sum_{k=0}^n \begin{bmatrix} \bar{h}_{(k,2)} \\ \bar{h}_{(k,3)} \end{bmatrix} = \begin{bmatrix} 0 \\ 0 \end{bmatrix}, \quad (2.5.17)$$

from which can be deduced that

$$\begin{bmatrix} \bar{h}_{(n,2)} \\ \bar{h}_{(n,3)} \end{bmatrix} = -\frac{1}{2} \left(\Delta^3 \begin{bmatrix} \tilde{F}_{RSS,2} \\ \tilde{F}_{RSS,3} \end{bmatrix} + \sum_{k=1}^{n-1} \tilde{s}_k^3 \begin{bmatrix} \tilde{F}_{k,2} \\ \tilde{F}_{k,3} \end{bmatrix} \right). \quad (2.5.18)$$

The next constraints are related to the bit orientation. From the definition, it follows that the inclination and azimuth at the bit are given by the angles θ_0 and ϕ_0 . The relative inclination is defined as the inclination difference between the inclination $\langle \Theta \rangle_{(1)}$ of chord $C_{(1)}$ and the inclination θ_0 of the bit leading to

$$\mathcal{H}_{(0,3)}(0) = \langle \Theta \rangle_{(1)} - \theta_0. \quad (2.5.19)$$

Analog to the inclination, the relative azimuth at the bit is defined by the azimuth $\langle \Phi \rangle_{(1)}$ of chord $C_{(1)}$ and the azimuth ϕ_0 of the bit. However, since the angles $\langle \Phi \rangle_{(1)}$ and ϕ_0 are defined in the (\vec{e}_1, \vec{e}_2) plane, an additional term is needed, which projects the BHA and the bit onto the plane (\vec{e}_1, \vec{e}_2) . This leads to the relation

$$\mathcal{H}_{(0,2)}(0) = \left(\langle \Phi \rangle_{(1)} - \phi_0 \right) \sin \langle \Theta \rangle_{(1)}. \quad (2.5.20)$$

By using (2.5.19) and (2.5.20), one can state that

$$\begin{bmatrix} \mathcal{H}_{(0,2)} \\ \mathcal{H}_{(0,3)} \end{bmatrix} (0) = \sum_{k=0}^n \begin{bmatrix} \bar{\mathcal{H}}_{(k,2)} \\ \bar{\mathcal{H}}_{(k,3)} \end{bmatrix} = \begin{bmatrix} \left(\langle \Phi \rangle_{(1)} - \phi_0 \right) \sin \langle \Theta \rangle_{(1)} \\ \langle \Theta \rangle_{(1)} - \theta_0 \end{bmatrix}, \quad (2.5.21)$$

from which another integration constant can be solved leading to

$$\begin{bmatrix} \bar{\mathcal{H}}_{(n,2)} \\ \bar{\mathcal{H}}_{(n,3)} \end{bmatrix} = \frac{3}{2} \left(\Delta^2 \begin{bmatrix} \tilde{F}_{RSS,3} \\ \tilde{F}_{RSS,2} \end{bmatrix} + \sum_{k=1}^{n-1} \tilde{s}_k^2 \begin{bmatrix} \tilde{F}_{k,3} \\ \tilde{F}_{k,2} \end{bmatrix} \right) + \begin{bmatrix} \left(\langle \Phi \rangle_{(1)} - \phi_0 \right) \sin \langle \Theta \rangle_{(1)} \\ \langle \Theta \rangle_{(1)} - \theta_0 \end{bmatrix}. \quad (2.5.22)$$

Now, all integration constants are found and expressed in (2.5.11), (2.5.12), (2.5.14), (2.5.15), (2.5.18) and (2.5.22) The deflection of the BHA at the $n - th$ stabilizer with respect to chord $C_{(1)}$ can be expressed as

$$\begin{bmatrix} \tilde{h}_{(n,2)} \\ \tilde{h}_{(n,3)} \end{bmatrix} (\lambda) = \sum_{k=2}^n \left[\begin{bmatrix} \langle \Theta \rangle_{(1)} - \langle \Theta \rangle_{(k)} \\ (\langle \Phi \rangle_{(1)} - \langle \Phi \rangle_{(k)}) \sin \langle \Theta \rangle_{(1)} \end{bmatrix} \lambda_{(k)}. \quad (2.5.23)$$

In this expression, the small angle approximation is used. This expression can be equated to the expression which follows from (2.5.9), which leads to

$$\begin{aligned} \begin{bmatrix} \tilde{h}_{(n,2)} \\ \tilde{h}_{(n,3)} \end{bmatrix} (\lambda) &= \lambda^3 \begin{bmatrix} \tilde{F}_{n,2} \\ \tilde{F}_{n,3} \end{bmatrix} - \begin{bmatrix} \frac{3}{8} \tilde{w} \lambda^4 \sin(\langle \Theta \rangle_{(1)}) \\ 0 \end{bmatrix} + \begin{bmatrix} \bar{\mathcal{H}}_{(n,3)} \\ \bar{\mathcal{H}}_{(n,2)} \end{bmatrix} \lambda + \begin{bmatrix} \bar{h}_{(n,2)} \\ \bar{h}_{(n,3)} \end{bmatrix} \\ &= \lambda^3 \begin{bmatrix} \tilde{F}_{n,2} \\ \tilde{F}_{n,3} \end{bmatrix} + \lambda \left[\begin{bmatrix} \langle \Theta \rangle_{(1)} - \theta_0 \\ (\langle \Phi \rangle_{(1)} - \phi_0) \sin \langle \Theta \rangle_{(1)} \end{bmatrix} - \begin{bmatrix} \frac{3}{8} \tilde{w} \lambda^4 \sin(\langle \Theta \rangle_{(1)}) \\ 0 \end{bmatrix} \right] \\ &+ \frac{1}{2} \left(\Delta^2 (3\lambda - \Delta) \begin{bmatrix} \tilde{F}_{RSS,2} \\ \tilde{F}_{RSS,3} \end{bmatrix} + \sum_{k=1}^{n-1} \left(\tilde{s}_k^2 (3\lambda - \tilde{s}_k) \begin{bmatrix} \tilde{F}_{k,2} \\ \tilde{F}_{k,3} \end{bmatrix} \right) \right). \end{aligned} \quad (2.5.24)$$

From this, the contact force at the last ideal stabilizer can be determined to be

$$\begin{aligned} \begin{bmatrix} \tilde{F}_{n,2} \\ \tilde{F}_{n,3} \end{bmatrix} &= -\frac{1}{\lambda^3} \sum_{k=1}^n \lambda_{(k)} \left[\begin{bmatrix} \langle \Theta \rangle_{(k)} - \theta_0 \\ (\langle \Phi \rangle_{(k)} - \phi_0) \sin \langle \Theta \rangle_{(1)} \end{bmatrix} + \begin{bmatrix} \frac{3}{8} \tilde{w} \lambda \sin(\langle \Theta \rangle_{(1)}) \\ 0 \end{bmatrix} \right] \\ &+ \frac{1}{2\lambda^3} \left(\Delta^2 (\Delta - 3\lambda) \begin{bmatrix} \tilde{F}_{RSS,2} \\ \tilde{F}_{RSS,3} \end{bmatrix} + \sum_{k=1}^{n-1} \left(\tilde{s}_k^2 (\tilde{s}_k - 3\lambda) \begin{bmatrix} \tilde{F}_{k,2} \\ \tilde{F}_{k,3} \end{bmatrix} \right) \right). \end{aligned} \quad (2.5.25)$$

It remains to find expressions for the contact forces at the non-ideal stabilizers. The integration constants which are found are similar to the those listed in [26]. The next section describes the derivation of the nonlinear complementary problem to find the contact forces at the non-ideal stabilizers.

2.5.1 Modelling of Non-Ideal Stabilizers

The contact forces at the non-ideal stabilizers depend on the deflection of the BHA at each stabilizer with respect to the borehole center. In order to find such an expression, first an expression for the last BHA segment is needed because the other segments depend on this expression recursively, as observed in (2.5.9).

To find this expression, the contact forces $\tilde{F}_{n,k}$ for $k = 2, 3$, found in (2.5.25) and the integration constants $\bar{h}_{(n,k)}$ and $\bar{\mathcal{H}}_{(n,k)}$ for $k = 2, 3$, from (2.5.18) and (2.5.22) are substituted in

the expression in (2.5.9) for $i = n$. This procedure leads to the concise formulation

$$\begin{aligned} \begin{bmatrix} \tilde{h}_{(n,2)} \\ \tilde{h}_{(n,3)} \end{bmatrix}(\tilde{s}) &= \begin{bmatrix} \langle \Theta \rangle_{(1)} - \theta_0 \\ (\langle \Phi \rangle_{(1)} - \phi_0) \sin(\langle \Theta \rangle_{(1)}) \end{bmatrix} \tilde{s} + \sum_{k=1}^n \zeta_k(\tilde{s}) \begin{bmatrix} \langle \Theta \rangle_{(1)} - \theta_0 \\ (\langle \Phi \rangle_{(k)} - \phi_0) \sin(\langle \Theta \rangle_{(k)}) \end{bmatrix} + \sum_{k=1}^{n-1} \zeta_{k+n}(\tilde{s}) \begin{bmatrix} \tilde{F}_{k,2} \\ \tilde{F}_{k,3} \end{bmatrix} \\ &+ \zeta_{2n}(\tilde{s}) \begin{bmatrix} \tilde{F}_{RSS,2} \\ \tilde{F}_{RSS,3} \end{bmatrix} + \zeta_{2n+1}(\tilde{s}) \begin{bmatrix} \sin(\langle \Theta \rangle_{(1)}) \\ 0 \end{bmatrix} \end{aligned} \quad (2.5.26)$$

with the functions $\zeta_i(\tilde{s})$, for $i = 1, 2, \dots, 2n + 1$, defined as

$$\zeta_k(\tilde{s}) := \frac{\tilde{s}^2(\tilde{s} - 3\lambda)}{2\lambda^3} \lambda_{(k)} \quad \text{for } k = 1, 2, \dots, n, \quad (2.5.27a)$$

$$\zeta_{k+n}(\tilde{s}) := \frac{\tilde{s}_k^2}{4\lambda^3} (\tilde{s}^2(3\lambda - \tilde{s})(\tilde{s}_k - 3\lambda) + 2\lambda^3(3\tilde{s} - \tilde{s}_k)) \quad \text{for } k = 1, 2, \dots, n-1, \quad (2.5.27b)$$

$$\zeta_{2n}(\tilde{s}) := \frac{\Delta^2}{4\lambda^3} (\tilde{s}^2(3\lambda - \tilde{s})(\Delta - 3\lambda) + 2\lambda^3(3\tilde{s} - \Delta)), \quad (2.5.27c)$$

$$\zeta_{2n+1}(\tilde{s}) := \frac{1}{16} \tilde{w} \tilde{s}^2 (-3\lambda + 2\tilde{s})(\lambda - \tilde{s}). \quad (2.5.27d)$$

Then, the deflection at stabilizer i for $i = 1, 2, \dots, n-1$, can be derived by evaluating (2.5.9) at $\tilde{s} = \tilde{s}_i$, resulting in

$$\begin{aligned} \begin{bmatrix} \tilde{h}_{i,2} \\ \tilde{h}_{i,3} \end{bmatrix} &:= \begin{bmatrix} \tilde{h}_{(i,2)} \\ \tilde{h}_{(i,3)} \end{bmatrix}(\tilde{s}_i) \\ &= \begin{bmatrix} \langle \Theta \rangle_{(1)} - \theta_0 \\ (\langle \Phi \rangle_{(1)} - \phi_0) \sin(\langle \Theta \rangle_{(1)}) \end{bmatrix} \tilde{s}_i + \sum_{k=1}^n \zeta_k(\tilde{s}_i) \begin{bmatrix} \langle \Theta \rangle_{(1)} - \theta_0 \\ (\langle \Phi \rangle_{(k)} - \phi_0) \sin(\langle \Theta \rangle_{(k)}) \end{bmatrix} \\ &+ \zeta_{2n}(\tilde{s}_i) \begin{bmatrix} \tilde{F}_{RSS,2} \\ \tilde{F}_{RSS,3} \end{bmatrix} + \zeta_{2n+1}(\tilde{s}_i) \begin{bmatrix} \sin(\langle \Theta \rangle_{(1)}) \\ 0 \end{bmatrix} + \sum_{k=1}^i \left(\zeta_{k+n}(\tilde{s}_i) \begin{bmatrix} \tilde{F}_{k,2} \\ \tilde{F}_{k,3} \end{bmatrix} \right) \\ &+ \sum_{k=i+1}^{n-1} \left(\zeta_{i+n}(\tilde{s}_k) \begin{bmatrix} \tilde{F}_{k,2} \\ \tilde{F}_{k,3} \end{bmatrix} \right). \end{aligned} \quad (2.5.28)$$

One should notice that this expression makes use of the following equality [26]:

$$\zeta_{k+n}(\tilde{s}_i) + \frac{1}{2} (\tilde{s}_k - \tilde{s}_i)^3 = \zeta_{i+n}(\tilde{s}_k), \quad \text{for } k > i. \quad (2.5.29)$$

The deflection of the stabilizer with respect to the borehole center is defined as $\vec{\delta}_i = [0 \quad \delta_{i,2} \quad \delta_{i,3}]^T \vec{I} = (\delta_i^I)^T \vec{I}$. The components of δ_i^I can be computed as

$$\begin{aligned} \begin{bmatrix} \delta_{i,2} \\ \delta_{i,3} \end{bmatrix} &:= \begin{bmatrix} \tilde{h}_{i,2} \\ \tilde{h}_{i,3} \end{bmatrix} - \sum_{k=2}^i \begin{bmatrix} \langle \Theta \rangle_{(1)} - \langle \Theta \rangle_{(k)} \\ (\langle \Phi \rangle_{(1)} - \langle \Phi \rangle_{(k)}) \sin(\langle \Theta \rangle_{(k)}) \end{bmatrix} \\ &= \sum_{k=1}^i \left(\zeta_{k+n}(\tilde{s}_i) \begin{bmatrix} \tilde{F}_{k,2} \\ \tilde{F}_{k,3} \end{bmatrix} \right) + \sum_{k=i+1}^{n-1} \left(\zeta_{i+n}(\tilde{s}_k) \begin{bmatrix} \tilde{F}_{k,2} \\ \tilde{F}_{k,3} \end{bmatrix} \right) + \begin{bmatrix} \tilde{q}_{i,2} \\ \tilde{q}_{i,3} \end{bmatrix} \end{aligned} \quad (2.5.30)$$

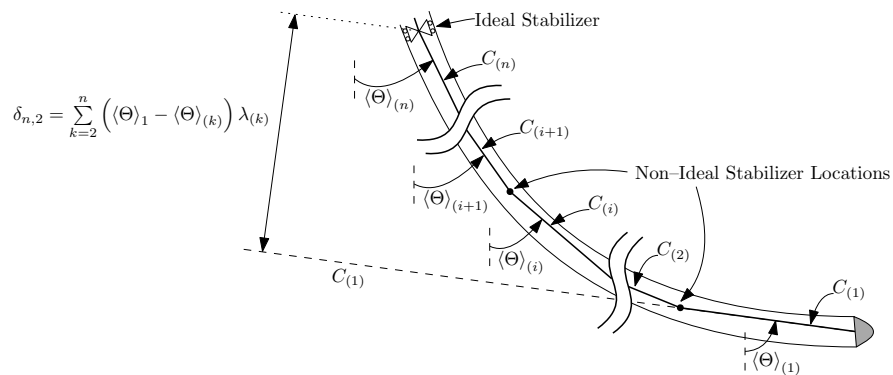


Figure 2.5.1: The last stabilizer is centered in the borehole, which defines a deflection for the last stabilizer as visualized. The drillstring, the non-ideal stabilizers and the RSS actuator are left out in this figure, which has been taken from [25].

where

$$\begin{aligned} \begin{bmatrix} \tilde{q}_{i,2} \\ \tilde{q}_{i,3} \end{bmatrix} &:= \sum_{k=1}^i \left(\lambda_{(k)} \begin{bmatrix} \langle \Theta \rangle_{(k)} - \theta_0 \\ (\langle \Phi \rangle_{(k)} - \phi_0) \sin(\langle \Theta \rangle_{(1)}) \end{bmatrix} \right) + \sum_{k=1}^n \left(\zeta_k (\tilde{s}_i) \begin{bmatrix} \langle \Theta \rangle_{(k)} - \theta_0 \\ (\langle \Phi \rangle_{(k)} - \phi_0) \sin(\langle \Theta \rangle_{(k)}) \end{bmatrix} \right) \\ &+ \zeta_{2n} (\tilde{s}_i) \begin{bmatrix} \tilde{F}_{RSS,2} \\ \tilde{F}_{RSS,3} \end{bmatrix} + \zeta_{2n+1} (\tilde{s}_i) \begin{bmatrix} \sin(\langle \Theta \rangle_{(1)}) \\ 0 \end{bmatrix}. \end{aligned} \quad (2.5.31)$$

The term which is subtracted in the first line of (2.5.30) represents the borehole center with respect to the reference configuration of the BHA at stabilizer i , visualized by Figure 2.5.1. By subtracting this term, the deflection with respect to the borehole center can be computed. This expression can be written concisely as

$$\underbrace{\begin{bmatrix} \delta_{1,2} \\ \vdots \\ \delta_{n-1,2} \\ \delta_{1,3} \\ \vdots \\ \delta_{n-1,3} \end{bmatrix}}_{\underline{\delta}} = K^{-1} \underbrace{\begin{bmatrix} \tilde{F}_{1,2} \\ \vdots \\ \tilde{F}_{n-1,2} \\ \tilde{F}_{1,3} \\ \vdots \\ \tilde{F}_{n-1,3} \end{bmatrix}}_{\underline{F}_k} + \underbrace{\begin{bmatrix} q_{1,2} \\ \vdots \\ q_{n-1,2} \\ q_{1,3} \\ \vdots \\ q_{n-1,3} \end{bmatrix}}_{\underline{q}}, \quad (2.5.32)$$

where K^{-1} is given by the inverse of (2.5.39).

All stabilizers have to comply with Signorini's contact law, which is an ideal unilateral contact law [13]. This law prevents the stabilizers from penetrating the borehole wall by imposing complementarity relations between the contact force and the contact distance. If the magnitude of the gap between a stabilizer and the borehole wall is denoted with M_g and

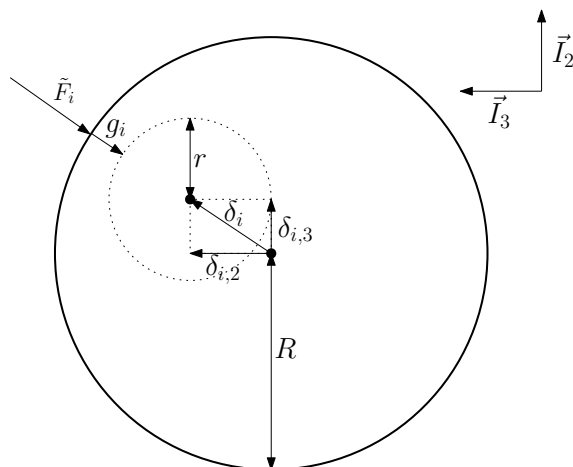


Figure 2.5.2: Visual representation of the gap variable at stabilizer i .

the magnitude of the contact force with M_F , then Signorini's contact law, which should hold for each individual stabilizer, states that

$$M_g \geq 0, \quad M_F \geq 0 \quad \text{and} \quad M_g M_F = 0. \quad (2.5.33)$$

The magnitudes of the contact forces are contained in a column $\underline{\Lambda} \in \mathbb{R}^{n-1}$. The direction of the contact force is determined by the gap variable g_i , for $i = 1, 2, \dots, n-1$, which indicates the closest distance between the borehole wall and the stabilizer i as visualized in Figure 2.5.2. In the case of a circular borehole, the gap variable $g_i(\underline{\delta})$ is a function of the deflection $\underline{\delta}_i$, which was defined in (2.5.30) and is defined as

$$g_i(\underline{\delta}_i) := (R - r) - \sqrt{\delta_{i,2}^2 + \delta_{i,3}^2} \quad \text{for } i = 1, 2, \dots, n-1, \quad (2.5.34)$$

in which R is the borehole radius, r the stabilizer radius and the difference between the two is the maximal clearance. The directional information of the contact forces is contained in a matrix \underline{W} , which is defined as

$$\underline{W} = \left(\frac{\partial g(\underline{\delta})}{\partial \underline{\delta}} \right)^\top, \quad (2.5.35)$$

where $\underline{g}(\underline{\delta})$ is a column containing all the gap variables g_i . The magnitudes of the contact forces are contained in a column $\underline{\Lambda} = [\Lambda_1 \dots \Lambda_{n-1}]^\top$. By combining the directional information

and the magnitudes, the contact forces can be written as

$$\underline{W}\underline{\Lambda} = \underbrace{\begin{bmatrix} -2\frac{\delta_{1,2}}{\sqrt{\delta_{1,2}^2+\delta_{1,3}^2}} & \cdots & 0 \\ \vdots & \ddots & \vdots \\ 0 & \cdots & -2\frac{\delta_{n-1,2}}{\sqrt{\delta_{n-1,2}^2+\delta_{n-1,3}^2}} \\ -2\frac{\delta_{1,3}}{\sqrt{\delta_{1,2}^2+\delta_{1,3}^2}} & \cdots & 0 \\ \vdots & \ddots & \vdots \\ 0 & \cdots & -2\frac{\delta_{n-1,3}}{\sqrt{\delta_{n-1,2}^2+\delta_{n-1,3}^2}} \end{bmatrix}}_{\underline{W}} \underbrace{\begin{bmatrix} \Lambda_1 \\ \vdots \\ \Lambda_{n-1} \end{bmatrix}}_{\underline{\Lambda}}. \quad (2.5.36)$$

By rewriting (2.5.32) and the relation $\underline{F}_k = \underline{W}\underline{\Lambda}$, the deflection can be written as

$$\underline{K}^* \underline{\delta} = \underline{Q} + \underline{W}\underline{\Lambda}, \quad (2.5.37)$$

with

$$\underbrace{\begin{bmatrix} K & \underline{0}_{n-1 \times n-1} \\ \underline{0}_{n-1 \times n-1} & K \end{bmatrix}}_{\underline{K}^*} \underbrace{\begin{bmatrix} \delta_{1,2} \\ \vdots \\ \delta_{n-1,2} \\ \delta_{1,3} \\ \vdots \\ \delta_{n-1,3} \end{bmatrix}}_{\underline{\delta}} = \underbrace{\begin{bmatrix} K & \underline{0}_{n-1 \times n-1} \\ \underline{0}_{n-1 \times n-1} & K \end{bmatrix}}_{\underline{Q}} \underbrace{\begin{bmatrix} q_{1,2} \\ \vdots \\ q_{n-1,2} \\ q_{1,3} \\ \vdots \\ q_{n-1,3} \end{bmatrix}}_{\underline{Q}} + \underline{W}\underline{\Lambda}, \quad (2.5.38)$$

where

$$K = \begin{bmatrix} \zeta_{n+1}(1) & \cdots & \zeta_{n+1}(\tilde{s}_i) & \cdots & \zeta_{n+1}(\tilde{s}_{n-1}) \\ \vdots & \ddots & \vdots & \ddots & \vdots \\ \zeta_{n+1}(\tilde{s}_i) & \cdots & \zeta_{n+i}(\tilde{s}_i) & \cdots & \zeta_{n+i}(\tilde{s}_{n-1}) \\ \vdots & \ddots & \vdots & \ddots & \vdots \\ \zeta_{n+1}(\tilde{s}_{n-1}) & \cdots & \zeta_{n+i}(\tilde{s}_{n-1}) & \cdots & \zeta_{2n-1}(\tilde{s}_{n-1}) \end{bmatrix}^{-1}. \quad (2.5.39)$$

The contact forces cannot be calculated by solving a LCP, as done in [26] and [29]. For an LCP formulation, two relations are needed, namely; (i) a linear equation expressing the gap's magnitude M_g as a function of the contact forces' magnitude $\underline{\Lambda}$ and the external forces' magnitude and; (ii) a complementarity relation as defined in (2.5.33). A necessity is that both the linear equation and the complementarity relation are written in terms of the magnitude of the gap and forces. The main obstacle to arrive to an LCP formulation is to write (2.5.37) in terms of the magnitudes, whilst preserving linearity between the magnitude variables. In [29], the author did derive such a linear equation on magnitude level. In that work,

however, a square borehole was considered rather than a circular one.

To compute the contact forces for a circular borehole a different approach is used. For a circular borehole, the relation between the magnitude of the contact forces and the magnitude of the gap is nonlinear. Hence, a nonlinear complementarity problem is considered. This nonlinear complementarity problem is solved via a proximal point approach which allows solving with efficient numerical methods. With the proximal point approach, the formulation of the unilateral contact law is converted into a proximal point formulation [1, 28]. In the following intermezzo, the concept of a proximal point is explained.

Intermezzo: Proximal Point

Consider a set C which contains all the possible values for a certain variable, which for this problem are all the non-negative reals: $C = \mathbb{R}^+$. Then, the proximal point $z = \text{prox}_{\mathbb{R}^+}(x)$ of a point x is the closest point from x to the set C , which is formulated as follows:

- if a point x is located in C , then the proximal point z is the point itself, i.e., $z = x$.
- if a point x is located outside of the set C , then the proximal point z is on the boundary of C . Then, two cases can be distinguished
 - if z is located on a smooth part of the boundary, then z is the proximal point for a outward ray to the set C starting in z .
 - if the point z lies on a non-smooth part of the boundary, then z is the proximal point for a whole cone of points constructed by the tangents to point z , starting at z .

In the remainder of this section, points z and x have no further meaning, but the concept of the proximal point formulation is used.

Signorini's contact law can be written in a proximal point formulation by the expression [28]:

$$\Lambda_i = \text{prox}_{\mathbb{R}^+}(\Lambda_i - rg_i) \quad \text{with } r > 0. \quad (2.5.40)$$

By evaluating this expression, one can conclude that this proximal point formulation is the same as the complementarity relation, namely

- if there is a contact force, the contact force is in the set \mathbb{R}^+ which means that the proximal point Λ_i equals the argument of the proximal point function. For this to be the case, the term rg_i should be zero. This can only be the case if the gap variable is zero since $r > 0$ implying $\Lambda_i > 0 \rightarrow \Lambda_i \in \text{interior}(\mathbb{R}^+) \rightarrow \Lambda_i = \text{prox}_{C_N}(\Lambda_i) \rightarrow g_i = 0$ since $r > 0$,
- if there is no contact force, the proximal point function should map to zero which is the case for all points $-rg_i \leq 0$. Since $r > 0$, this should imply that $g_i \geq 0$. $\Lambda_i = 0 \rightarrow 0 = \text{prox}_{C_N}(-rg_i), r > 0 \rightarrow 0 = \text{prox}_{\mathbb{R}^+}(-rg_i), r > 0 \rightarrow g_i \geq 0$ since $r > 0$.

Thus, the contact forces in this nonlinear complementarity problem can be computed using the proximal point formulation. In this formulation, the contact forces are calculated using

the proximal point function (2.5.40), for $i = 1, 2, \dots, n - 1$, where the input arguments depends on the gap function defined in (2.5.34) which contains the nonlinearity. The gap function is subject to the equation for the deflection defined in (2.5.37).

2.6 Borehole Propagation Model

The differential equation governing the propagation of the borehole can be obtained by combining the model components. From the force equilibrium, defined in (2.5.2) and (2.5.3), an expression can be found for the forces and moments at the bit after substitution of the contact forces at the last stabilizer, in (2.5.25). This procedure leads to the expressions

$$\begin{aligned} \begin{bmatrix} \tilde{F}_{0,2} \\ \tilde{F}_{0,3} \end{bmatrix} &= \begin{bmatrix} -\tilde{F}_{RSS,2} - \sum_{k=1}^n \tilde{F}_{k,2} + \tilde{w}\lambda \sin \langle \Theta \rangle_{(1)} \\ -\tilde{F}_{RSS,3} - \sum_{k=1}^n \tilde{F}_{k,3} \end{bmatrix} \\ &= -\frac{1}{2\lambda^3} (2\lambda^3 + \Delta^3 - 3\lambda\Delta^2) \begin{bmatrix} \tilde{F}_{RSS,2} \\ \tilde{F}_{RSS,3} \end{bmatrix} - \frac{1}{2\lambda^3} \left(\sum_{k=1}^{n-1} 2\lambda^3 + \tilde{s}_k^3 - 3\lambda\tilde{s}_k^2 \begin{bmatrix} \tilde{F}_{k,2} \\ \tilde{F}_{k,3} \end{bmatrix} \right) \\ &\quad + \frac{1}{\lambda^3} \left(\sum_{k=1}^n \lambda^{(k)} \begin{bmatrix} \langle \Theta \rangle_{(k)} - \theta_0 \\ (\langle \Phi \rangle_{(k)} - \phi_0) \sin \langle \Theta \rangle_{(1)} \end{bmatrix} \right) + \begin{bmatrix} \frac{5}{8}\tilde{w}\lambda \sin(\langle \Theta \rangle_{(1)}) \\ 0 \end{bmatrix}, \end{aligned} \quad (2.6.1)$$

$$\begin{aligned} \begin{bmatrix} \tilde{M}_{0,2} \\ \tilde{M}_{0,3} \end{bmatrix} &= \begin{bmatrix} -\Delta\tilde{F}_{RSS,3} - \sum_{k=1}^n \tilde{s}_k \tilde{F}_{k,3} \\ \Delta\tilde{F}_{RSS,2} + \sum_{k=1}^n \tilde{s}_k \tilde{F}_{k,2} - \frac{1}{2}\tilde{w}\lambda^2 \sin \langle \Theta \rangle_{(1)} \end{bmatrix} \\ &= \frac{\Delta}{2\lambda^2} (2\lambda - \Delta) (\lambda - \Delta) \begin{bmatrix} -\tilde{F}_{RSS,3} \\ \tilde{F}_{RSS,2} \end{bmatrix} + \frac{1}{2\lambda^2} \left(\sum_{k=1}^{n-1} \tilde{s}_k (2\lambda - \tilde{s}_k) (\lambda - \tilde{s}_k) \begin{bmatrix} -\tilde{F}_{k,3} \\ \tilde{F}_{k,2} \end{bmatrix} \right) \\ &\quad - \frac{1}{\lambda^2} \left(\sum_{k=1}^n \lambda^{(k)} \begin{bmatrix} -(\langle \Phi \rangle_{(k)} - \phi_0) \sin \langle \Theta \rangle_{(1)} \\ \langle \Theta \rangle_{(k)} - \theta_0 \end{bmatrix} \right) - \begin{bmatrix} 0 \\ \frac{1}{8}\tilde{w}\lambda^2 \sin(\langle \Theta \rangle_{(1)}) \end{bmatrix}. \end{aligned} \quad (2.6.2)$$

The equations for the forces and moments at the bit are expressed in frame \vec{I} . The expression obtained from the bit/rock interface is expressed in \vec{i} . Since the difference between the angles related to \vec{I} and \vec{i} is small, the transformation matrix $A_{Ii}(\Phi, \phi, \Theta, \theta)$, given in (2.4.3), is close to identity. Therefore the equations expressed (2.6.1) and (2.6.2) are substituted directly into (2.6.3) and (2.6.11), without any transformation.

The equation obtained for the moment at the bit \vec{M}_0 is substituted into (2.4.14), leading

to the differential equation

$$\begin{bmatrix} \frac{d\phi}{d\xi} \sin(\theta) \\ \frac{d\theta}{d\xi} \end{bmatrix} = \frac{1}{\Pi\chi} \begin{bmatrix} \cos(\varsigma) & -\sin(\varsigma) \\ -\sin(\varsigma) & -\cos(\varsigma) \end{bmatrix}^{-1} \begin{bmatrix} \tilde{M}_{0,2} \\ \tilde{M}_{0,3} \end{bmatrix}. \quad (2.6.3)$$

The inverse of the matrix in (2.6.3) is always defined since the determinant is equal to 1 irrespective of ς . Hence, from (2.6.3) can be deduced that $\frac{d\phi}{d\xi} \sin(\theta)$ is determined to be

$$\begin{aligned} \frac{d\phi}{d\xi} \sin(\theta) &= \sum_{k=1}^n a_k \left(c_\varsigma \left(\langle \Phi \rangle_{(k)} - \phi_0 \right) \sin \langle \Theta \rangle_{(1)} + s_\varsigma \left(\langle \Theta \rangle_{(k)} - \theta_0 \right) \right) \\ &+ \sum_{k=1}^{n-1} b_k \left(s_\varsigma \tilde{F}_{k,2} + c_\varsigma \tilde{F}_{k,3} \right) + c_1 \left(s_\varsigma \tilde{F}_{RSS,2} + c_\varsigma \tilde{F}_{RSS,3} \right) + s_\varsigma c_2 \sin \langle \Theta \rangle_{(1)}, \end{aligned} \quad (2.6.4)$$

in which the abbreviations $c_\varsigma = \cos \varsigma$ and $s_\varsigma = \sin \varsigma$ are used, and the term $\frac{d\theta}{d\xi}$ is determined to be

$$\begin{aligned} \frac{d\theta}{d\xi} &= \sum_{k=1}^n a_k \left(c_\varsigma \left(\langle \Theta \rangle_{(k)} - \theta_0 \right) - s_\varsigma \left(\langle \Phi \rangle_{(k)} - \phi_0 \right) \sin \langle \Theta \rangle_{(1)} \right) \\ &+ \sum_{k=1}^{n-1} b_k \left(c_\varsigma \tilde{F}_{k,2} - s_\varsigma \tilde{F}_{k,3} \right) + c_1 \left(c_\varsigma \tilde{F}_{RSS,2} - s_\varsigma \tilde{F}_{RSS,3} \right) + c_\varsigma c_2 \sin \langle \Theta \rangle_{(1)}, \end{aligned} \quad (2.6.5)$$

where,

$$a_k = \frac{\lambda^{(k)}}{\lambda^2 \Pi\chi}, \quad (2.6.6)$$

$$b_k = -\frac{\tilde{s}_k}{2\lambda^2 \Pi\chi} (2\lambda - \tilde{s}_k) (\lambda - \tilde{s}_k), \quad (2.6.7)$$

$$c_1 = -\frac{\Delta}{2\lambda^2 \Pi\chi} (2\lambda - \Delta) (\lambda - \Delta), \quad (2.6.8)$$

$$c_2 = \frac{1}{8\Pi\chi} \tilde{w} \lambda^2, \quad (2.6.9)$$

where the contact forces $\tilde{F} = \underline{W}\underline{\Lambda}$ are found by solving the system of equations in (2.5.40) and (2.5.34), subject to the linear relations (2.5.37). The coefficients in (2.6.6) - (2.6.9) are similar to [25] when it is assumed that $\epsilon = \frac{\xi}{\eta}$.

The derivative of the average borehole inclinations $\langle \Theta \rangle'_{(i)}$ and azimuths $\langle \Phi \rangle'_{(i)}$ for $i = 1, 2, \dots, n$, is given by

$$\frac{d\langle \Theta \rangle'_{(i)}(\xi)}{d\xi} = \frac{\Theta_{i-1} - \Theta_i}{\lambda_{(i)}}, \quad \frac{d\langle \Phi \rangle'_{(i)}(\xi)}{d\xi} = \frac{\Phi_{i-1} - \Phi_i}{\lambda_{(i)}}, \quad (2.6.10)$$

which are the ξ -derivatives of (2.3.2) and (2.3.3).

Expressions for the inclination Θ_0 and azimuth Φ_0 of the borehole at the bit can be found by substituting (2.4.4) in (2.4.13) and rewriting these expressions to

$$\begin{bmatrix} \psi_2 \\ \psi_3 \end{bmatrix} = \frac{1}{\eta\Pi} \begin{bmatrix} \cos(\varpi) & \sin(\varpi) \\ -\sin(\varpi) & \cos(\varpi) \end{bmatrix}^{-1} \begin{bmatrix} \tilde{F}_{0,2} \\ \tilde{F}_{0,3} \end{bmatrix}. \quad (2.6.11)$$

In this equation, the inverse of the matrix is always defined since the determinant is equal to 1. Using this expression, one can derive Θ_0 to be

$$\begin{aligned} \Theta_0 = & \theta_0 - \frac{c_\varpi \tilde{F}_{0,2} - s_\varpi \tilde{F}_{0,3}}{\eta\Pi} \\ & \theta_0 + \sum_{k=1}^n \bar{a}_k \left(c_\varpi \left(\langle \Theta \rangle_{(k)} - \theta_0 \right) - s_\varpi \left(\langle \Phi \rangle_{(k)} - \phi_0 \right) \sin \langle \Theta \rangle_{(1)} \right) \\ & + \sum_{k=1}^{n-1} \bar{b}_k \left(c_\varpi \tilde{F}_{k,2} - s_\varpi \tilde{F}_{k,3} \right) + \bar{c}_1 \left(c_\varpi \tilde{F}_{RSS,2} - s_\varpi \tilde{F}_{RSS,3} \right) + \bar{c}_2 c_\varpi \sin \langle \Theta \rangle_{(1)} \end{aligned} \quad (2.6.12)$$

and $\sin(\langle \Theta \rangle_{(1)})\Phi_0$ to be

$$\begin{aligned} \sin(\langle \Theta \rangle_{(1)})\Phi_0 = & \sin(\langle \Theta \rangle_{(1)})\phi_0 - \frac{s_\varpi \tilde{F}_{0,2} + c_\varpi \tilde{F}_{0,3}}{\eta\Pi} \\ & \sin(\langle \Theta \rangle_{(1)})\phi_0 + \sum_{k=1}^n \bar{a}_k \left(s_\varpi \left(\langle \Theta \rangle_{(k)} - \theta_0 \right) + c_\varpi \left(\langle \Phi \rangle_{(k)} - \phi_0 \right) \sin \langle \Theta \rangle_{(1)} \right) \\ & + \sum_{k=1}^{n-1} \bar{b}_k \left(s_\varpi \tilde{F}_{k,2} + c_\varpi \tilde{F}_{k,3} \right) + \bar{c}_1 \left(s_\varpi \tilde{F}_{RSS,2} + c_\varpi \tilde{F}_{RSS,3} \right) + \bar{c}_2 s_\varpi \sin \langle \Theta \rangle_{(1)} \end{aligned} \quad (2.6.13)$$

with coefficients

$$\bar{a}_k = -\frac{\lambda_{(k)}}{\eta\Pi\lambda^3}, \quad (2.6.14)$$

$$\bar{b}_k = \frac{1}{2\eta\Pi} \left(2\lambda^3 + \tilde{s}_k^3 - 3\lambda\tilde{s}_k^2 \right), \quad (2.6.15)$$

$$\bar{c}_1 = \frac{1}{2\eta\Pi} \left(2\lambda^3 + \Delta^3 - 3\lambda\Delta^2 \right), \quad (2.6.16)$$

$$\bar{c}_2 = -\frac{5\tilde{w}\lambda}{8\eta\Pi}. \quad (2.6.17)$$

These coefficients are the same as in [25].

To concisely formulate the borehole propagation model, a summary of the leading equations

is given. The borehole propagation model is given by the set of delay differential equations namely

$$\frac{d\phi}{d\xi} \sin(\theta) = \sum_{k=1}^n a_k \left(c_\varsigma \left(\langle \Phi \rangle_{(k)} - \phi_0 \right) \sin \langle \Theta \rangle_{(1)} + s_\varsigma \left(\langle \Theta \rangle_{(k)} - \theta_0 \right) \right) \quad (2.6.18)$$

$$+ \sum_{k=1}^{n-1} b_k \left(s_\varsigma \tilde{F}_{k,2} + c_\varsigma \tilde{F}_{k,3} \right) + c_1 \left(s_\varsigma \tilde{F}_{RSS,2} + c_\varsigma \tilde{F}_{RSS,3} \right) + s_\varsigma c_2 \sin \langle \Theta \rangle_{(1)}$$

$$\frac{d\theta}{d\xi} = \sum_{k=1}^n a_k \left(c_\varsigma \left(\langle \Theta \rangle_{(k)} - \theta_0 \right) - s_\varsigma \left(\langle \Phi \rangle_{(k)} - \phi_0 \right) \sin \langle \Theta \rangle_{(1)} \right) \quad (2.6.19)$$

$$+ \sum_{k=1}^{n-1} b_k \left(c_\varsigma \tilde{F}_{k,2} - s_\varsigma \tilde{F}_{k,3} \right) + c_1 \left(c_\varsigma \tilde{F}_{RSS,2} - s_\varsigma \tilde{F}_{RSS,3} \right) + c_\varsigma c_2 \sin \langle \Theta \rangle_{(1)},$$

$$\frac{d \langle \Theta \rangle_{(i)}(\xi)}{d\xi} = \frac{\Theta_{i-1} - \Theta_i}{\lambda_{(i)}}, \quad \frac{d \langle \Phi \rangle_{(i)}(\xi)}{d\xi} = \frac{\Phi_{i-1} - \Phi_i}{\lambda_{(i)}}. \quad (2.6.20)$$

with coefficients, $a_k, k = 1, \dots, n$ in (2.6.6), $b_k, k = 1, \dots, n-1$ in (2.6.7), c_1 in (2.6.8), and c_2 in (2.6.9). The output equations of the system, being the inclination and azimuth at the bit, are derived to be

$$\Theta_0 = \theta_0 + \sum_{k=1}^n \bar{a}_k \left(c_\varpi \left(\langle \Theta \rangle_{(k)} - \theta_0 \right) - s_\varpi \left(\langle \Phi \rangle_{(k)} - \phi_0 \right) \sin \langle \Theta \rangle_{(1)} \right) \quad (2.6.21)$$

$$+ \sum_{k=1}^{n-1} \bar{b}_k \left(c_\varpi \tilde{F}_{k,2} - s_\varpi \tilde{F}_{k,3} \right) + \bar{c}_1 \left(c_\varpi \tilde{F}_{RSS,2} - s_\varpi \tilde{F}_{RSS,3} \right) + \bar{c}_2 c_\varpi \sin \langle \Theta \rangle_{(1)},$$

$$\sin(\langle \Theta \rangle_{(1)}) \Phi_0 = \sin(\langle \Theta \rangle_{(1)}) \phi_0 + \sum_{k=1}^n \bar{a}_k \left(s_\varpi \left(\langle \Theta \rangle_{(k)} - \theta_0 \right) + c_\varpi \left(\langle \Phi \rangle_{(k)} - \phi_0 \right) \sin \langle \Theta \rangle_{(1)} \right) \quad (2.6.22)$$

$$+ \sum_{k=1}^{n-1} \bar{b}_k \left(s_\varpi \tilde{F}_{k,2} + c_\varpi \tilde{F}_{k,3} \right) + \bar{c}_1 \left(s_\varpi \tilde{F}_{RSS,2} + c_\varpi \tilde{F}_{RSS,3} \right) + \bar{c}_2 s_\varpi \sin \langle \Theta \rangle_{(1)}.$$

with coefficients, $\bar{a}_k, k = 1, \dots, n$ in (2.6.14), $\bar{b}_k, k = 1, \dots, n-1$ in (2.6.15), \bar{c}_1 in (2.6.16), and \bar{c}_2 in (2.6.17). In both the differential equations (2.6.18) - (2.6.20) as well as the output equations (2.6.21) and (2.6.22) the contact forces are calculated based on the NCP which is written as in a proximal point formulation. The proximal point formulation solves simultaneously the following set of equations:

$$\Lambda_i = \text{prox}_{\mathbb{R}^+}(\Lambda_i - r g_i) \quad \text{with } r > 0, \quad (2.6.23)$$

$$g_i(\underline{\delta}_i) := (R - r) - \sqrt{\delta_{i,2}^2 + \delta_{i,3}^2} \quad \text{for } i = 1, 2, \dots, n - 1, \quad (2.6.24)$$

$$\underline{K}^* \underline{\delta} = \underline{Q} + \underline{W}\underline{\Lambda}. \quad (2.6.25)$$

with \underline{K}^* and \underline{Q} defined in .

The model which is obtained is a so-called delay differential equations subject to set-valued force laws for the unilateral contact of non-ideal stabilizers. The delay nature stems from the fact that the deflection of the BHA depends on the historical values of its orientation. The unilateral contact law stems from the fact that the stabilizers in the borehole have to comply with Signorini's contact law.

3 Analysis of Borehole Propagation Model

This chapter presents the analyses of the borehole propagation model that has been developed in Chapter 2. The first analysis is a verification of the derived model by comparison with the results in [26] as described in Section 3.1. Recall that [26] is a two-dimensional model. Subsequently, the effect and validation of the extension to three dimensions is made. Also the onset of oscillations which potentially could lead to borehole spiraling are discussed in this section. Then in Section 3.2, the effect of the inclusion of the non-ideal stabilizers is shown by altering the diameter of the borehole. Lastly, in Section 3.3, a potential use case of the model is presented by considering a certain actuation path.

In these analyses, a so-called benchmark model is considered, taken from [25]. This model is a two-stabilizer model, which implies that the BHA has one ideal stabilizer at the end (at the interface with the drill-string) and one non-ideal stabilizer. The length of the segments is $\ell_{(i)} = 3.66\text{m}$, for $i = 1, 2$. The RSS actuator is located 0.6m behind the bit. The parameters which characterize the behavior of the BHA are the distributed weight $w = 1.08 \cdot 10^3 \frac{\text{N}}{\text{m}}$ and the flexural stiffness $EI = 7.2 \cdot 10^6 \text{Nm}^2$. The active weight on the bit is chosen in the interval $W \in [20, 45]\text{kN}$. The RSS actuator has actuation limits of $\pm 16\text{kN}$. The maximum distance between the stabilizer and the overgaged borehole, referred to as the clearance R^* , is the radius of the borehole R minus the radius of the stabilizer r . The clearance is within the interval $R^* \in [0.1, 1] \cdot 10^{-2}\text{m}$. In practice, this clearance varies over the borehole length ξ . In this analysis, however, a constant clearance over the evolution variable ξ is considered.

Scaling these parameters following the scaling described in Section 2.4.3, leads to a BHA segment length $\lambda_{(i)} = 1$ for $i = 1, 2$, where the RSS actuation pads are located on $\Delta = \frac{1}{6}$ behind the bit. Scaling of the lengths also implies that the scaled maximum clearance is $\tilde{R}^* \in [0.27, 2.7] \cdot 10^{-3}$. To reduce complexity, in the analysis, the maximum clearance of $\tilde{R}^* = 0.01$ for the non-ideal stabilizer. Based on the characteristic force $F^* = 1.61 \cdot 10^3\text{kN}$, the distributed weight on the BHA is determined to be $\tilde{w} = 2.45 \cdot 10^{-3}$. The active weight, characteristic force and the parameter choice for the bit yield to the dimensionless group $\eta\Pi \in [3.7, 8.37] \cdot 10^{-1}$. The RSS actuation limits scale to be $\pm 10^{-2}$. Furthermore, the dimensionless parameter ϵ is defined to be $\epsilon = \frac{\chi}{\eta}$ which is measure of the relative difficulty to impose an angular penetration to the bit with respect to a lateral penetration. This parameter is chosen to be $\epsilon = 0.1$. An overview of all the (scaled) variables is shown in Table 3.1.

Table 3.1: The variables and their scaled counterparts used in the analyses.

Description	Variable	Value [unit]	Scaled Equivalent	Value
Segment Length	$\ell_{(i)}$	3.66 [m]	$\lambda_{(i)}$	1
Position RSS actuation	-	0.6 [m]	Δ	$\frac{1}{6}$
Distributed weight	w	$1.08 \cdot 10^3 \frac{N}{m}$	\tilde{w}	$2.45 \cdot 10^{-3}$
Flexural stiffness	EI	$7.2 \cdot 10^6 [Nm^2]$	-	-
Active weight on bit	W	[20,45] [kN]	$\eta\Pi$	$[3.7, 8.37] \cdot 10^{-1}$
Actuation limits	-	$\pm 16\text{kN}$	-	$\pm 10^{-2}$
Maximum clearance	R^*	$[0.1, 1] \cdot 10^{-2} [m]$	\tilde{R}^*	$[0.27, 2.7] \cdot 10^{-3}$

The simulations are done with a numerical scheme in Matlab Simulink. This numerical scheme is built up based on the derived equations as depicted in Figure 3.0.1. The model computes the derivatives θ_0 and $\sin(\Theta)\phi_0$ of the inclination and azimuth using (2.6.4) and (2.6.5) and integrates these with respect to evolution variable ξ . The model output equations (2.6.12) and (2.6.13) are calculated to infer Θ_0 and Φ_0 . Then these values are stored and used to compute their delayed variants required in the computation of the average inclination $\langle\Theta\rangle_{(i)}$ and average azimuth $\langle\Phi\rangle_{(i)}$. The model makes use of a ODE45 solver with variable step sizes. This step size is chosen such that the relative and absolute tolerance are met which are both set at 10^{-12} .

The contact forces are calculated using the proximal point formulation as described in subsection 2.5.1. Numerically, this is solved using a fixed point iteration. In a fixed point iteration, the algorithm searches for a solution x such that $x_{k+1} = g(x_k)$ where $g(x)$ is a system of nonlinear equations. Implementation of this numerical method leads to the Algorithm 1. One should notice that the proximal point function can be seen as max function of the input argument $\Lambda_i - rg_i$ and zero.

3.1 Validation of the model

Validation of the model can be numerically performed by comparing a 2D-scenario taken from [25] with the simulation results given by the 3D-model. If the parameters ς and ϖ are chosen such that the off-diagonal terms in (2.6.3) and (2.6.11) are zero, then the behavior in the Θ direction is independent from the behavior in the Φ direction and vice versa. This scenario can be obtained by choosing $\varsigma = 0$ and $\varpi = 0$. Then, considering the (x, z) -plane should yield the output for Θ_0 and the contact forces for $\frac{d\theta}{d\xi}$ and ψ_2 .

The scenario which is considered is a borehole which initially starts vertically, thus $\Theta_0 = 0$ [rad] and $\theta_0 = 0$ [rad]. Since only the (x, z) -plane is considered, the azimuths are set to zero, thus $\Phi_0 = 0$ [rad] and $\phi_0 = 0$ [rad]. At $\xi = 1$, there is a step in actuator force $\tilde{F}_{RSS,2}$ from 0

Algorithm 1 Fixed-point iteration to solve the nonlinear complementarity problem for the case of one non-ideal stabilizer.

Assume $\Lambda = 0$
 Calculate deflection for $\Lambda = 0$ based on (2.5.37)
 Calculate gap based on (2.5.34)
if $g_1 > 0$ **then**
 $\tilde{F}_1 = 0$
else
 Calculate W based on (2.5.36)
 iteration variable $j = 0$
 while Λ not converged **do**
 $j = j+1$
 Calculate deflection based on (2.5.37)
 Calculate gap based on (2.5.34)
 Calculate $\Lambda_1 = \max(\Lambda_1 - r \cdot g_1, 0)$
 error $\Lambda_i(j) - \Lambda_i(j-1)$
 if error < tolerance **then**
 Λ_i is converged
 $\tilde{F}_1 = \underline{W}\Lambda$
 else
 Λ_1 not converged
 end if
 end while
end if

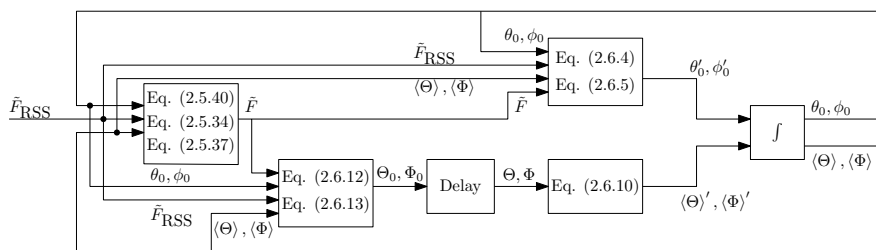


Figure 3.0.1: The setup of the numerical scheme used to compute the response of the borehole propagation model. In this scheme the columns $\Theta := [\Theta_0, \dots, \Theta_n]^T \in \mathbb{R}^{n+1}$ and $\Phi := [\Phi_0, \dots, \Phi_n]^T \in \mathbb{R}^{n+1}$ account for the delayed borehole inclinations and azimuths. The parameters $\langle \Theta \rangle := [\langle \Theta \rangle_{(1)}, \dots, \langle \Theta \rangle_{(n)}]^T \in \mathbb{R}^n$ and $\langle \Phi \rangle := [\langle \Phi \rangle_{(1)}, \dots, \langle \Phi \rangle_{(n)}]^T \in \mathbb{R}^n$ represent the average inclination and azimuths.

to $2 \cdot 10^{-2}$. The simulation is compared for three different scenarios by altering $\eta\Pi$. In Figure 3.1.1, the response of the system is shown for $\eta\Pi = 0.5$, $\eta\Pi = 0.2$ and $\eta\Pi = 0.05$, up to the borehole length $\xi = 10$. In [25], it is stated that the short length scale response corresponds to the first unit length in ξ after application of the step in RSS force. In the simulation, the step in actuation force happens at $\xi = 1$, which implies that the short length scale is for $1 \leq \xi < 2$. The delay terms Θ_i and Φ_i for $i = 1, 2$, are all constant in the short length scale. As a consequence, the borehole evolution is then a solution of a non-delay complementarity system for $\xi < 1$.

The medium length scale, ranging from $2 \leq \xi\lambda + 1$ starts when the first non-ideal stabilizer passes through the kink created by the RSS actuation at $\xi = 1$ and runs until all stabilizers have passed through this initial kink. For each $\xi = \tilde{s}_i + 1$ for $i = 1, 2, \dots, n$, a stabilizer passes through the initial kink. The stabilizer induces a new kink in the borehole curvature at the bit, creating a discontinuity in the inclination (and azimuth). This discontinuity, due to the geometric feedback, could lead to self-induced oscillations. After all stabilizers have passed through the kink, its effect diminishes, and the borehole evolves along a borehole with a constant curvature and asymptotically along a constant inclination [25].

As aforementioned, these simulations are also done in [25] with an identical result which validates the derived model in this work, at least partially. The simulations and a linear (local) stability analysis in [25] evidently show the occurrence of a Hopf-bifurcation depending on the variable $\eta\Pi$. A Hopf-bifurcation happens when the first pair of complex poles passes through the imaginary axis, leading to oscillations in the borehole trajectory being amplified or suppressed. For this scenario, it has been numerically determined in [25] that a Hopf-bifurcation happens for a critical value of $\eta\Pi$, namely $\eta\Pi^* = 0.147$, meaning that at least one pair of complex poles is in the complex right half plane for $\eta\Pi < \eta\Pi^*$.

The top plot of Figure 3.1.1, for $\eta\Pi = 0.5 \gg \eta\Pi^*$ shows that the oscillations damp out fast, since no oscillation is observed in the borehole trajectory. This is because the complex poles are far into the complex left half plane (CLHP). In this case, the non-ideal stabilizer only has contact with the upper borehole wall since the contact force is smaller than 0.

The middle plot, for $\eta\Pi = 0.2$ which is closer to the point where Hopf-bifurcation happens, shows oscillations which do damp out over the increasing borehole length. These oscillations are present since complex pair of poles are all located fairly close to the imaginary axis, but are still in the CLHP. Also in this scenario, one can notice that the stabilizer only contacts the upper wall, also showing an oscillatory contact force.

The bottom plot shows the scenario where $\eta\Pi = 0.05 \ll \eta\Pi^*$. As a consequence, the response of the system is growing in an oscillatory fashion. Since bit tilt saturation is not included in the derived model, this oscillations grows unbounded, which is unrealistic. This oscillation is the consequence of at least one complex pair of poles being in the complex right

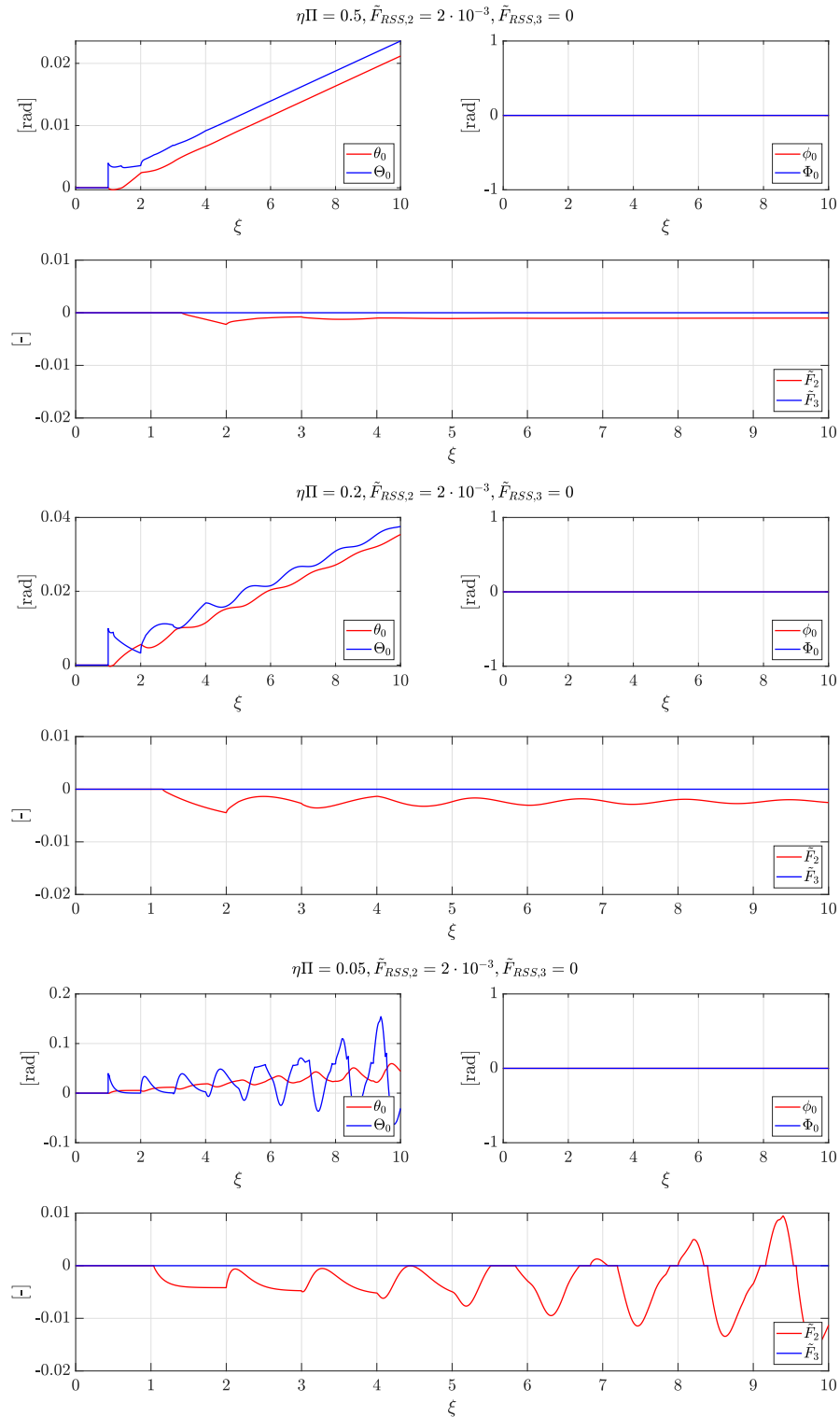


Figure 3.1.1: Response of the model to a step in RSS force for respectively $\eta\Pi = 0.5$, $\eta\Pi = 0.2$ and $\eta\Pi = 0.05$ and $\varsigma = 0$ and $\varpi = 0$.

half plane. In the plot of the contact forces, one can see that the stabilizer starts bouncing between the top and bottom borehole wall. During a bounce between the top and the bottom, the contact force is constant at zero which implies that the complementarity relation imposed, holds. When the contact forces starts to increase or decrease again, the stabilizer is in contact with the wall. These oscillations could lead to borehole spiraling. In this simulations this does not happen since the bit-tilt is not saturated, which allows the bit-tilt to grow unbounded. If the bit-tilt is saturated, the growth of the oscillations is bounded which could lead to a limit cycle, which is known as borehole spiraling.

Furthermore, on the short length scale, these simulations show the discontinuities induced by the stabilizer moving through the initial kink, at $\xi = [2, 3]$ since the step in RSS actuation force takes place at $\xi = 1$ and $\lambda_{(1)} = \lambda_{(2)} = 1$. Later on in the response, these discontinuities vanish if the oscillations also damp out which is the case for $\eta\Pi = 0.5$ and $\eta\Pi = 0.2$. In the case where the oscillations start to grow, the discontinuities tend to grow along, which is the case for $\eta\Pi = 0.05$. It can be seen that for these scenarios the azimuth Φ is independent of the behavior of the inclination Θ . Since there is no external loading in all cases, i.e., $\tilde{F}_{RSS,3} = 0$, this results in the azimuth staying constant at zero.

Both the model derived in this thesis as the simulations in [25], have the same output for the borehole inclination Θ_0 and the contact force $\tilde{F}_{RSS,2}$. Besides that, the model derived in this thesis is capable of predicting instability correctly based on the parameter group $\eta\Pi$, in line with to the results found in [25]. This is important in order to predict borehole spiraling. Based on these fact, the model is assumed to be validated, when it concerns the inclination Θ without bit walk and bit flip.

The next goal of this section is to validate whether the model outputs the correct azimuths Φ_0 and corresponding contact forces $\tilde{F}_{RSS,3}$. The validation is done in a similar fashion, thus also for $\eta\Pi = 0.5$, $\eta\Pi = 0.2$ and $\eta\Pi = 0.05$. It is assumed that the flexural stiffness of the drillstring in all directions is the same. Furthermore, the same Euler-Bernoulli equation applies. Besides that, the external loading in both directions is the same, apart from the loading due to gravity. Lastly, the step in RSS actuation is similar $\tilde{F}_{RSS,2} = \tilde{F}_{RSS,3} = 2 \cdot 10^{-2}$. Together, this should imply that the response in both directions should be identical if the distributed loading due to gravity is assumed to be zero, i.e., $\tilde{w} = 0$, under the condition that $\varsigma = 0$ and $\varpi = 0$. In Figure 3.1.2, it can be seen that it is indeed the case that the behavior in both directions is identical which implies that the model is validated.

A more involved aspect in the comparison between a 2D model and a 3D model is the existence of bit walk and bit flip in the 3D model. The bit walk is an imposed angle between the lateral forces of the bit and the lateral penetration at the bit which implies, for example, that a contact force \tilde{F}_2 contributes to the behavior of both the inclination and azimuth. The bit flip is a change in orientation between the plane in which the moment on the bit occurs and the plane in which the bit changes orientation. This implies that the behavior of

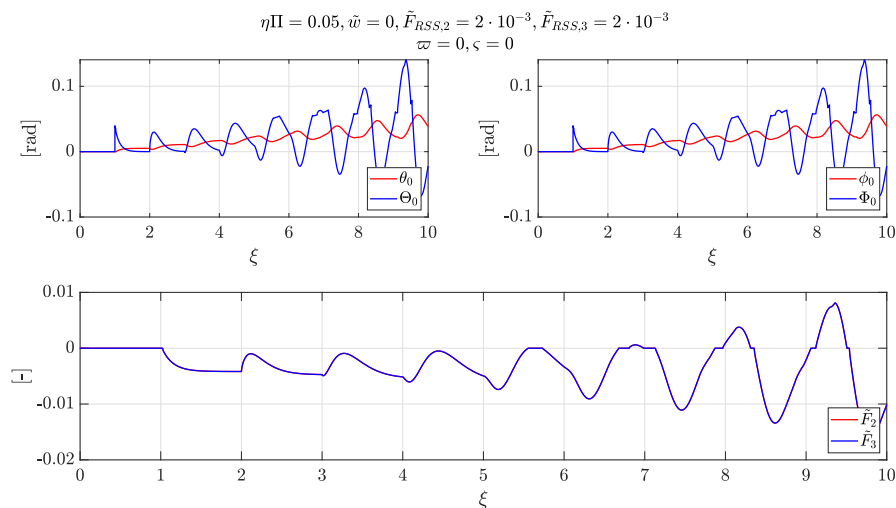


Figure 3.1.2: Response of the model to a step in RSS actuation force in both directions, thus $\tilde{F}_{RSS,2} = \tilde{F}_{RSS,3} = 2 \cdot 10^{-2}$ where $\tilde{w} = 0$.

both directions do interfere with each other, resulting in a more complex borehole evolution. In Figure 3.1.3, the same experiment as previously described is conducted, this time with gravity, i.e., $\tilde{w} = 2.45 \cdot 10^{-3}$ to show the effect of the bit walk and bit flip. For this scenario, both the bit flip and bit walk are chosen to be $\varsigma = \varpi = -15$ deg. This simulation shows that the response in both directions is again oscillatory, similar to those in Figure 3.1.1, but now there forms a phase delay between the variables in the two directions. It would make sense that this is caused by the bit walk and bit flip since these are the two altered parameters. A more in depth analysis on the bit walk and bit flip parameters is out of the scope of this thesis.

3.2 Effect of Non-Ideal Stabilizers

The implementation of the non-ideal stabilizers leads to differences in behavior compared to borehole propagation models that only contain ideal stabilizers. In the case of an ideal stabilizer, the stabilizer always makes contact with the borehole wall. The inclusion of non-ideal stabilizers, also introduces different scenarios which each have their different behavior. To analyze this effect, a simulation is ran of different values for the maximal borehole clearance, namely $\tilde{R}^* \in \{0, 1, 1.5, 2\} \cdot 10^{-3}$. The case where $\tilde{R}^* = 0$, implies that the non-ideal stabilizer has no clearance and thus behaves as an ideal stabilizer. The outcome of this simulation is taken as baseline. The clearance is varied to see the effect of a larger borehole. The simulation is, again, based on a initially vertical borehole, with a step in $F_{RSS,2} = F_{RSS,3}$ from 0 to $0.7 \cdot 10^{-3}$ in actuator force at $\xi = 1$. In Figure 3.2.1, the borehole inclination and the azimuth at the bit, the bit tilt and the contact forces as a function of ξ , are displayed. By enlarging the borehole, the BHA tends to bend more. This larger bending is a consequence

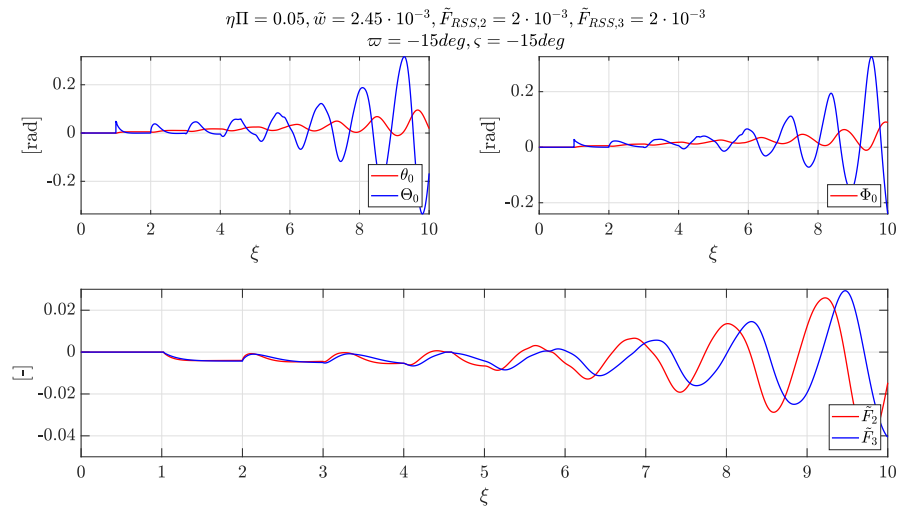


Figure 3.1.3: Response of the model to a step in RSS actuation force in both directions, thus $\tilde{F}_{RSS,2} = \tilde{F}_{RSS,3} = 2 \cdot 10^{-2}$. Also $\varsigma = \varpi = -15$ deg.

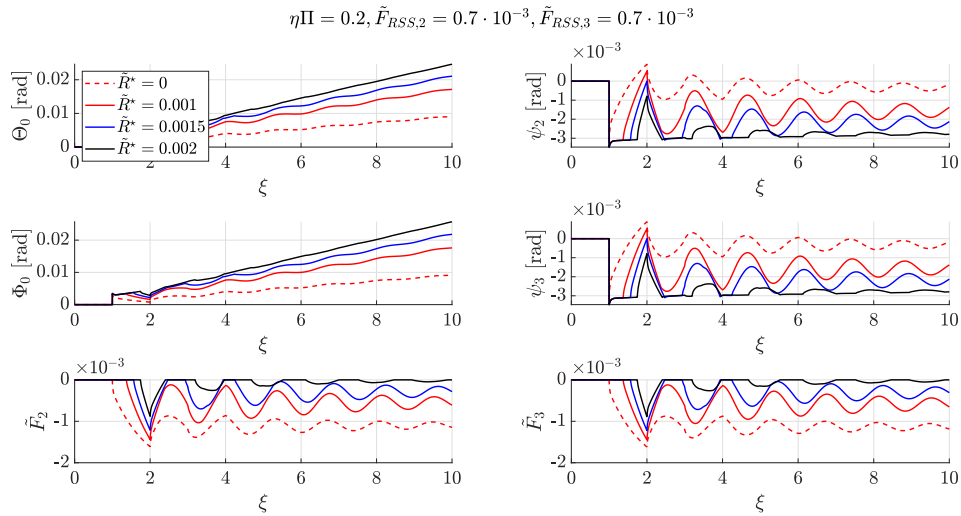


Figure 3.2.1: The effect of varying the maximum clearance to see the effect of the inclusion of the non-ideal stabilizers.

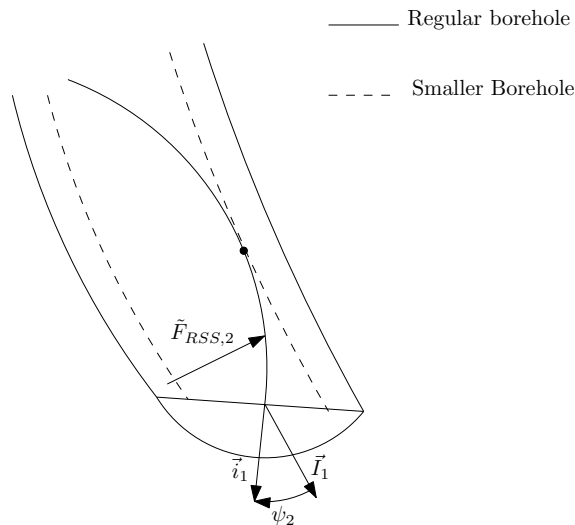


Figure 3.2.2: This figure visualizes that the BHA tends to bend more when the borehole radius is larger, i.e., it takes longer for the stabilizer to hit the borehole wall.

of the stabilizer traveling further before it contacts the borehole wall which is visualized in Figure 3.2.2. This is evidenced by the results in Figure 3.2.1, which show that, for a larger \tilde{R}^* , the non-ideal stabilizers contacts the borehole wall for the first time at a larger distance ξ . Consequently, the bit tilt becomes larger for a larger \tilde{R}^* , which, in turn, leads to a larger growth of Θ_0 and θ_0 . For $\tilde{R}^* = 0.0015$ and $\tilde{R}^* = 0.002$, the BHA behaves as a one stabilizer model in the intervals at which the contact force is zero. In conclusion, non-ideal stabilizers affect the response of directional drilling systems significantly. It can both affect the constant tendency and also the oscillatory response. Keeping in mind that in practice any stabilizer exhibits more clearance, embedding these elements is of crucial importance in the understanding of drilling processes.

3.3 Potential Usage of Derived Borehole Propagation Model

The way in which directional drilling is currently controlled is by sending command messages, containing desired inclinations, to the RSS based on downhole measurements [19]. This desired inclination is converted into a constant RSS actuation force which is subsequently applied by the RSS actuator. Studies have shown that a constant actuation force could lead to a borehole that evolves with a constant curvature and, asymptotically, with a constant inclination, under the condition that the length scale is sufficiently long [25]. In practice, deviations from the desired trajectory can happen for various reasons including rock variations, bit wear and actuator imperfections. These deviations have to be corrected manually in an open-loop fashion at the drill rig by an operator. In order to take these deviations

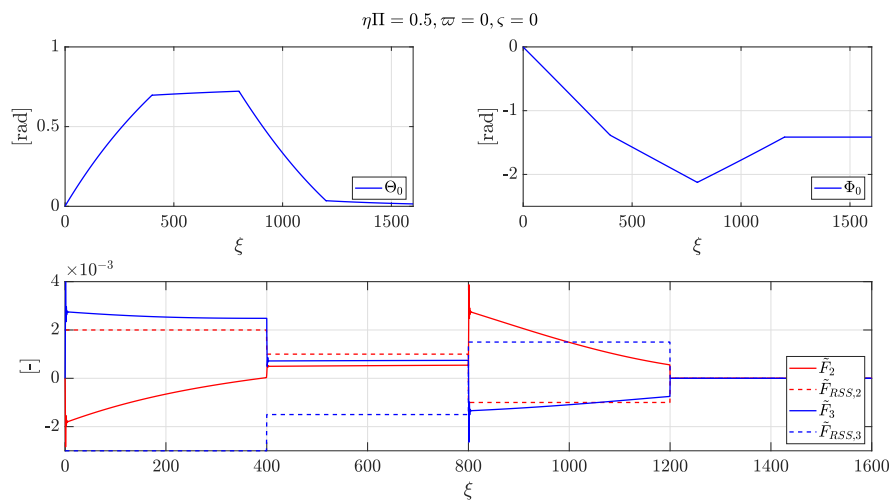


Figure 3.3.1: The long range response to an actuation path. The dashed lines indicate the actuation path which is applied. This path is different in the two directions. For this simulation, $\varpi = 0deg$].

into account, the borehole propagation model can be used to predict the trajectory of the borehole under a constant RSS actuation force. This prediction can be used by an operator or to compute what actuation force should be applied to correct. By a sequence of different actuation forces, the borehole can be steered into any desired direction.

An RSS actuation path is designed to see what the long time response is to several actuation steps. This path consist of several sections at which the actuation in one direction is constant, respectively $\tilde{F}_{RSS,2} \in \{2, 1, -1, 0\} \cdot 10^{-3}$ and $\tilde{F}_{RSS,3} \in \{-3, -1.5, 1.5, 0\} \cdot 10^{-3}$. In Figure 3.3.1, the response to this path of actuation is shown. In this plot, also the actuation path itself is shown. In this analysis, the borehole clearance is chosen as $R = 1 \cdot 10^{-3}$. At each instant where there is a step in actuation which is at $\xi \in \{0, 400, 800, 1200\}$, the model shows oscillations which damp out since $\eta\Pi = 0.2 > \eta\Pi^*$ with $\eta\Pi^*$ the critical value of $\eta\Pi$ at which the Hopf-bifurcation occurs. After the oscillations have damped out, the borehole shows a constant curvature as expected from [25]. This simulation shows that the contact forces change with a increasing borehole length depending on the inclination and azimuth at that borehole depth. Furthermore, it can be seen that the contact forces tend to decrease in magnitude during the period of constant curvature. In the last section, where there is no actuation force, there is also no contact force, implying that the non-ideal stabilizer does not contact the borehole wall.

In conclusion, the derived borehole propagation model is a function of BHA parameters, bit parameters, borehole clearance and the RSS actuation force. The model is capable of predicting the long term behavior of the borehole evolution. Eventually for the purpose of reaching a desired location in an open-loop fashion, the ‘inverse’ model could be used, that

takes a desired path or target as input and outputs the RSS actuator force that realizes the desired path or target. Examples of such scenarios can be found in [26]. In addition, the current model could be used to design model-based feedback controllers with the aim to track a desired path in an autonomous fashion, as done in [7, 19, 27].

3.4 Discussion

This chapter described the analysis which was done with the model. The first step was a validation step by numerical comparison of a step in RSS actuation force to the 2D-model of [25]. This step showed that the 3D model can be viewed as two 2D models by choosing the right bit walk and bit flip. It has been shown that the model behaves exactly the same as in [25] for the considered scenarios, which validates both the inclination and azimuth directions. Furthermore, it has been shown that the model is capable of predicting the onset of oscillations depending on the key model parameter for $\eta\Pi$. Based on the parameter $\eta\Pi$, these oscillations damp out or grow unbounded, potentially leading to borehole spiraling. The oscillations grow unbounded, if the bit-tilt is not saturated. Subsequently, by altering the parameter controlling the maximum clearance between the non-ideal stabilizer and the borehole wall, the borehole evolution altered both in the constant tendency as in the oscillatory behavior. Lastly, the analysis showed that it is capable of predicting the long term behavior under application of a constant RSS force.

4 Conclusion and Recommendations

This section describes the conclusions which can be drawn from this thesis based on the objectives formulated in Chapter 1 and also discusses recommendations for further extensions and analysis of the model.

4.1 Conclusions

The first goal was to derive a three-dimensional model for borehole propagation. This model should be an extension of the model B with the inclusion of non-ideal stabilizers. The non-ideal stabilizer account for a realistic scenario because the size of the stabilizers in general does not match the size of the borehole radius. The second objective was to perform a numerical study in order to validate the model by comparison with results in [25]. Thirdly, the goal was to perform a numerical study which predict the onset of oscillations in a 3D scenario.

The results of the first research objective is a borehole propagation model that includes any number of non-ideal stabilizers. This model is in analytical form, and can predict the azimuth and inclination as response of system as a function of the actuation parameters. There are three model components which constitute the borehole propagation model. The first is a bit-rock interface component which relates the forces and moments acting on the bit to the rock penetration and bit tilt following from this. The second component relates the kinematics of the bit to the evolution of the borehole geometry. Lastly, a static BHA model which relates external loading as well as constraints imposed by the stabilizers to the forces and moments acting on the bit. These components combined form the borehole propagation model. The derived model falls in the class of nonlinear delay complementarity systems. The delay comes from the fact that the the deformation of the BHA depends on the current and delayed borehole inclinations and azimuth, i.e., the shape of the drilled borehole. The complementarity relations stem from the fact that the non-ideal stabilizers have to comply with Signorini's unilateral contact law.

The main contribution of this work is in the modeling of non-ideal stabilizers in the three-dimensional case. The calculation of contact forces was previously done by [25] for the two-dimensional case using the framework of linear complementarity systems. In the three-dimensional case, non-ideal stabilizers were previously modeled by [29]. The authors, how-

ever, considered the intersection of the borehole to be square which deviates from the circular/ellipsoidal shape of a borehole in reality. In order to model non-ideal stabilizers, the more generic framework of nonlinear complementarity problems is considered. This because, the magnitude of the gap between the non-ideal stabilizer and the borehole wall does not attain a linear relationship with the magnitude of the forces experienced by the non-ideal stabilizer. In a nonlinear complementarity problem, the relation between the magnitude of the gap variable and the magnitude of the contact forces can remain nonlinear and is completed by complementarity relations following from Signorini's unilateral contact law.

The second objective was to validate the derived model by comparison with numerical results from the two-dimensional model in [25], particularly, the borehole inclination and contact forces for various scenarios. To compare the 2D model with the 3D model from this work, the inclination and azimuth direction need to be decoupled. This can be done by choosing the appropriate values for the bit walk and the bit flip. This way, the 3D model becomes a set of two 2D models. The model derived in this work predicts exactly the same borehole inclination as the model from [25], which implies that the model for the inclination is validated. Furthermore, the azimuth direction was validated by comparison to the inclination direction. With the same external loading, which implies excluding gravity, both the inclination and azimuth direction should yield the same output variables. This was also proven to be correct and with that, the model is validated.

The last objective was to perform a numerical study which predict the onset of oscillations that lead to borehole spiraling. In [25] is stated that self-induced oscillations, for example by an step in actuation force, can possibly lead to borehole spiraling. To show these self-induced oscillations, the evolution of the borehole after a step in actuation force is simulated for different values for a key dimensionless group. These simulations showed the occurrence of a Hopf-bifurcation based on the location of the pair of complex poles. The presence of this complex pair of poles is the reason the system starts oscillating and stems from the geometric feedback that the stabilizers receive from the borehole walls. If the key dimensionless group is larger than a critical value determined in [25], the oscillations damp out, meaning borehole spiraling does not occur. If the key dimensionless group is smaller than the critical value, then the oscillations grow unbounded. In [25], is shown that these unbounded oscillations converge to a limit cycle with the inclusion of the bit-tilt saturation. The bit-tilt saturation prevents the oscillations from growing unbounded. In conclusion, the model is able to predict the onset of oscillations, which either damp out or grow unbounded depending on a key dimensionless group.

Next, the influence of the non-ideal stabilizer was studied by comparing the response of the borehole propagation model with non-ideal stabilizer to a model with ideal stabilizers. Simulations showed that the BHA tends to bend more, because the stabilizer travels longer before hitting the borehole wall. After the step in RSS is made, it takes longer for the stabilizer to reach the borehole wall which means that the contact forces is zero for a longer period

of time. As a consequence, the bit-tilt increases for a wider borehole, which leads to a larger growth of inclination and azimuth. Therefore, it is concluded that the borehole evolution is significantly influenced by the inclusion of the non-ideal stabilizers.

Lastly, the long-range behavior of the borehole propagation model was studied. It is concluded that the model response tends to an inclination and azimuth that increase/decrease with an almost constant rate if the RSS actuation force is kept constant.

The borehole propagation model extends existing models by the inclusion of non-ideal stabilizers via the framework of nonlinear complementarity problems. In particular, we showed that the modeling of non-ideal stabilizers significantly affects the borehole evolution and are, therefore, crucial for the understanding of the directional drilling processes. One of the usages of this model is to predict the RSS force required to realize a certain borehole trajectory. Another usage is to serve for model-based feedback controller design with the aim to accurately track borehole trajectory. One of the usages of this model is to predict what the actuation force needs to be in order to follow a certain trajectory. The other usage is to design model-based feedback controllers which could lead the BHA to a target faster and more accurate.

4.2 Recommendations

The first natural recommendation is to include bit-tilt saturation in the model formulation. As aforementioned, bit-tilt saturation is an important aspect in borehole spiraling as it allows capturing borehole spiraling, rather than only predicting the onset, as shown in literature. The numerical studies show that the oscillations in the inclination and azimuth grow unrealistically unbounded, which allows to only partially predict the borehole evolution. With the inclusion of bit-tilt saturation, the model can potentially also capture the evolution of steady-state oscillation, related to borehole spiraling. Similar to non-ideal stabilizer, the bit-tilt saturation is also described by set-valued force laws. Therefore, it is expected that a similar modeling approach based on nonlinear complementarity problems can be utilized to model bit-tilt saturation.

The second recommendation for future work is to analyze further what the effect of the bit walk and bit flip is on the evolution of the borehole. As shown in the numerical studies, these parameters create a delay between the response of the inclination Θ and the azimuth Φ . How this delay relates to these variables should be investigated. Besides the effect of the walk bit and the bit flip, a qualitative analysis should be done to identify classes of solutions and their stability. This analyses could be done analytically as done previously in literature.

Thirdly, the model should be used in the design of a model-based controller. If the drilling of a desired path could be done autonomously, this would reduce costs of directional drilling

since the operator is not necessary anymore. Also this model-based controller could be used to make directional drilling faster and to avoid the occurrence of borehole spiraling. Then, the objective should be to robustly track a pre-specified borehole path, whilst rippling and spiraling is avoided. To design a controller based on a nonlinear complementarity system is an open challenge.

Lastly, a comparison should be done with field data to further validate the model. In this comparison, one could see if the model is representative enough to model reality. An important aspect of this is the prediction of borehole spiraling. It is important to check whether or not the model can predict these oscillations correctly, such that they can possibly be prevented by changing the design or the model-based controller. Such a comparison should be done in cooperation with the industry.

Bibliography

- [1] V. Acary, B. Brogliato *Numerical Methods for Nonsmooth Dynamical Systems: Applications in Mechanics and Electronics* Springer Verlag, 35, pp.526, 2008, Lecture Notes in Applied and Computational Mechanics, 978-3-540-75391-9
- [2] M.H. Amara, *Use of Drillstring Models and Data Bases for the Scientific Control of Vertical and Directional Hole Paths*, Proc. SPE/IADC Drilling Conf., SPE-13495-MS, New Orleans, Louisiana, USA, March 1985.
- [3] J.J.B. Biemond, W. Michiels, N. van de Wouw, *Stability analysis of equilibria of linear delay complementarity systems*, IEEE Control Systems Letters, Vol. 1, Issue 1, pp. 158–163, July 2017.
- [4] M. Birades, R. Fenoul, *A Microcomputer Program for Prediction of Bottomhole Assembly Trajectory*, SPE Drilling Engineering, Vol. 3, Issue 2, pp. 31–38, SPE-15285-PA, Silver-Creek, CO, USA, June 1988.
- [5] N.P. Callas, R.L. Callas, *Boundary value problem is solved*, Oil Gas J., Vol. 78, No. 50, pp. 62–66, 1980.
- [6] D.C.K. Chen, M. Wu, *State-of-the-Art BHA Program Produces Unprecedented Results*, Proc. Int. Petroleum Technol. Conf. (IPTC), Kuala Lumpur, Malaysia, December 2008.
- [7] Demirer , Nazli , Zalluhoglu , Umut , Marck, Julien , Darbe , Robert , Morari , Manfred *Autonomous Directional Drilling with Rotary Steerable Systems*, 2019 American Control Conference (ACC), 2019, pp. 5203-5208, doi: 10.23919/ACC.2019.8814644.
- [8] G.C. Downton, M. Ignova, *Stability and Response of Closed Loop Directional Drilling System using Linear Delay Differential Equations*, Proc. IEEE Int. Conf. Control Appl. (CCA), pp. 893–898, Denver, CO, USA, September 2011.
- [9] F.J. Fischer, *Analysis of Drillstrings in Curved Boreholes*, Proc. 49th Annu. Fall Meeting Soc. Petroleum Eng. of AIME, p. SPE 5071, Dallas, Texas, USA, October 1974.
- [10] B. Graham, W. Reilly, *Deep Water: The Gulf Oil Disaster and the Future of Offshore Drilling*, National Commission on the BP Deepwater Horizon Oil Spill and Offshore Drilling, January 2011.
- [11] R.C. Hibbeler, *Engineering Mechanics: Statics*, 14th Edition, Pearson, 2016.

-
- [12] H. King, *Horizontal Drilling & Directional Drilling: Natural Gas Wells*, Retrieved from <http://geology.com/articles/horizontal-drilling/>, Web, November 2020.
- [13] Leine, R. I., Wouw, van de, N, *Stability and convergence of mechanical systems with unilateral constraints*. (Lecture notes in applied and computational mechanics; 2008; Vol. 36). Springer. <https://doi.org/10.1007/978-3-540-76975-0>
- [14] A. Lubinski, H.B. Woods *Factors affecting the angle of Inclination and Dog-Legging in Rotary Bore Holes* American Petroleum Institute, Mid-Continent District, 1953
- [15] J. Marck, *A Nonlinear Dynamical Model of Borehole Spiraling*, PhD dissertation, Faculty of the Graduate School of the University of Minnesota, Minneapolis, Minnesota, USA, December 2015.
- [16] J. Marck, E. Detournay, A. Kuesters,, J. Wingate, *Analysis of Spiraled-Borehole Data by Use of a Novel Directional-Drilling Model*, SPE Drilling & Completion, vol. 29, no. 3, pp. 267–278, Fort Worth, Texas, USA, March 2014.
- [17] K. Millheim, *The Effect Of Hole Curvature On The Trajectory Of A Borehole*, Proc. 52nd Annu. Fall Tech. Conf. Exhibit. Soc. Petroleum Eng. AIME, Denver, CO, USA, pp. 1–8, October 1977.
- [18] K. Millheim, S. Jordan, C.J. Ritter, *Bottom-Hole Assembly Analysis Using the Finite-Element Method*, J. Petroleum Technol., Soc. Petroleum Eng. vol. 30, no. 2, pp. 256–274, February 1978.
- [19] N. van de Wouw, F.H.A. Monsieurs, E. Detournay, *Dynamic state-feedback control of nonlinear three-dimensional directional drilling systems*, Proceedings of the 10th IFAC Symposium on Nonlinear Control Systems (NOLCOS), Monterey, CA, USA, August 2016.
- [20] M. Neubert, G. Heisig, *Mathematical description of the directional drilling process and simulation of directional control algorithm*, Zeitschrift Angew. Math. Mech., Vol. 76, No. 5, pp. 361–362, January 1996.
- [21] P.E. Pastusek, V.J. Brackin, *A Model for Borehole Oscillations*, SPE Annual Technical Conference and Exhibition, No. SPE 84448, Denver, Colorado, USA, October 2003.
- [22] L. Perneder, J. Marck, E. Detournay, *A Model of Planar Borehole Propagation*, SIAM J. Appl. Math., Vol. 77, Issue 4, pp. 1089–1114, 2017.
- [23] L. Perneder, *A Three-Dimensional Mathematical Model of Directional Drilling*, Ph.D. dissertation, Faculty of the Graduate School of the University of Minnesota, Minneapolis, Minnesota, USA, January 2013.
- [24] S. Rafie, H.S. Ho, and U. Chandra, *Applications of a BHA Analysis Program in Directional Drilling*, Proc. IADC/SPE Drilling Conf., pp. 345–354, Dallas, TX, USA, February 1986.
-

-
- [25] M. F. Shakib, *Nonlinear Modeling for Dynamic Analysis of Directional Drilling Processes*, M.Sc. Thesis D&C 2017.095, Eindhoven University of Technology, The Netherlands, 2017.
- [26] M.F. Shakib, E. Detournay, N. van de Wouw *Nonlinear dynamic modeling and analysis of borehole propagation for directional drilling* International Journal of Non-Linear Mechanics, number 113, 2019, doi: <https://doi.org/10.1016/j.ijnonlinmec.2019.01.014>
- [27] O. Villareal, *Robust output-feedback control of 3D directional drilling systems*, M.Sc. dissertation, Delft University of Technology, Delft, The Netherlands, July 2016.
- [28] N. van de Wouw *An introduction to Time-Stepping: a Numerical Technique for Mechanical Systems with Unilateral Constraints* Eindhoven University of Technology, The Netherlands,
- [29] U. Zalluhoglu, J.Marck, H. Gharib, Y. Zhao, *Borehole Propagation with Undergaged Stabilizers: Theory and Validation* Journal of Dynamic Systems, Measurement and Control, Transactions of the ASME, Vol. 141, Issue 5, 2019
- [30] Y. Zhao, U. Zalluhoglu, J. Marck, N. Demirer, M. Morari *Model Predictive Control for Mud Motor Operation in Directional Drilling* 2019 American Control Conference (ACC), 2019, doi: 10.23919/ACC.2019.8815289

Declaration concerning the TU/e Code of Scientific Conduct for the Master's thesis

I have read the TU/e Code of Scientific Conductⁱ.

I hereby declare that my Master's thesis has been carried out in accordance with the rules of the TU/e Code of Scientific Conduct

Date

07-04-21 (seventh of september 2021)

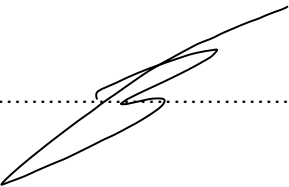
Name

Harmen Berksen

ID-number

1011277

Signature



Submit the signed declaration to the student administration of your department.

ⁱ See: <http://www.tue.nl/en/university/about-the-university/integrity/scientific-integrity/>

The Netherlands Code of Conduct for Academic Practice of the VSNU can be found here also.

More information about scientific integrity is published on the websites of TU/e and VSNU